University of Glasgow
DEPARTMENT OF
AEROSPACE
ENGINEERING

Hybrid Mesh Generation Techniques and Euler Flow Solver Validation

Y.F.Yao

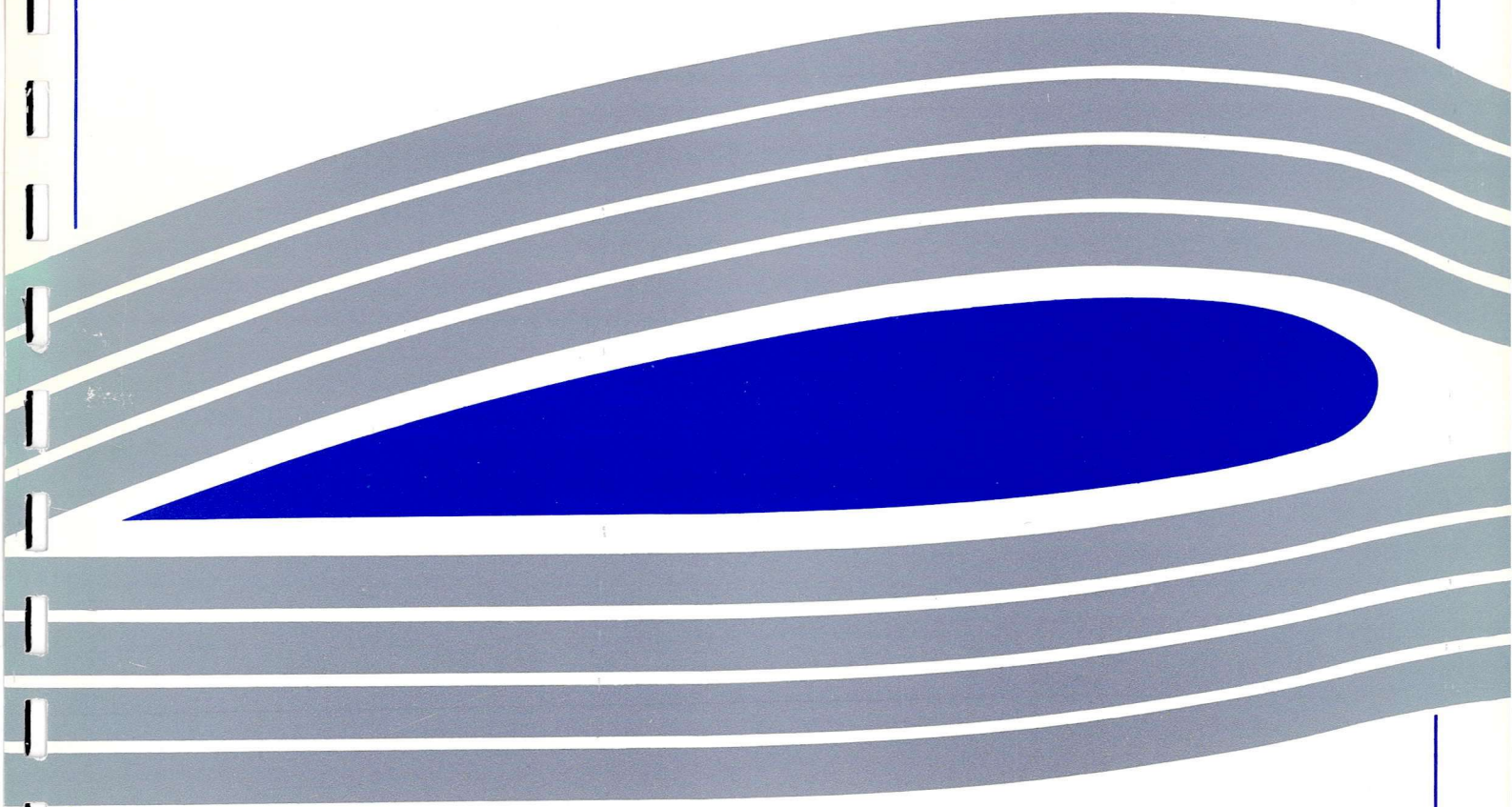

Hybrid Mesh Generation Techniques and Euler Flow Solver Validation

Y.F.Yao

Dept. of Aerospace Engineering
Aero. Report 9501
University of Glasgow

Jan.10,1995

Hybrid Mesh Generation Techniques and Euler Flow Solver Validation

Y.F.Yao
Dept. of Aerospace Engineering
University of Glasgow

Abstracts

Mesh generation is an important aspect in Computational Fluid Dynamics(CFD). Methods based on the structured and unstructured meshes both have their advantages and disadvantages. The best way is to combine them and adopt the benefits of both. The unstructured mesh which has shown the potential power to deal with the complex geometry will encounter problems in dealing with the viscous flow case. In this paper we first discuss some methods to generate both structured and unstructured meshes. An Euler flow solver with a cell-centered, finite-volume, Point-Gauss-Seidel implicit time-stepping scheme is validated on these two types of mesh topology. Then we propose a strategy, called the "SKIN" method, to construct a hybrid mesh based on structured and unstructured meshes. The Euler flow solver is then modified and applied on this type of hybrid mesh. Numerical tests demonstrate the efficiency of the hybrid mesh, generated by the present method, and the robustness of the particular Euler solver on different type of meshes.

Keyword: CFD, mesh generation technique, Euler solver

1. Introduction

Within the field of computational fluid dynamics, mesh generation has been considered as an important aspect for continued development and research. Considerable efforts have been made in this area over years and impressive progress has been achieved[1].

One question arising from numerical flow simulation is which approach to mesh generation is superior: that based on structured curvilinear systems of points, giving rise to a quadrilateral mesh in two dimensions and a hexahedral mesh in three dimensions, respectively; or the approach of an unstructured assembly of triangles in two dimensions or tetrahedra in three dimensions. The capabilities of both approaches has been demonstrated. The advantages and disadvantages of one method over the other has been discussed in ref.[2]. Generally the advantages of the structured mesh approach are (1) the flexibility for implementation of all

classes of flow algorithm; (2) efficient utilization of the vector architecture of computers; (3) efficient use of CPU time and computer memory; (4) a good enviroment for the multigrid technique. The disadvantages include (1) lack of total flexility for very complicated geometries; (2) not generally amenable to mesh adaptivity. In contrast the unstructured method (1) is flexible for very complicated geometries; (2) is a natural enviroment for mesh adaption; (3) is most suitable for transient computations in which adaptivity to moving flow features is essential. Some disadvantages include (1) not necessarily amenable for all classes of flow algorithms, and to the implementation of multigrid; (2) relatively inefficient in computer memory requirements. It is very interesting to note that the advantages of one approach are the disadvantages of another. Thus it is possible to achieve a unified approach which could take advantage of the different grid procedures.

Another point is that the unstructured grid, although has been used very successfully for inviscid flow simulation, is still problematic when applied to viscous flow simulations. In general, the boundary layer region of the fluid close to solid walls need to be discretised using cells with aspect ratio of the order of thousands. This requirement is partly based on the physical aspects of the boundary layer near the wall, where rapid changes take place in the direction normal to the streamline flow, and partly from the fact that a grid with adequate resolution across the boundary layer, but maintainning a small aspect ratio, will need considerable computer resources. Therefore to resolve viscous flows involving boundary layers with cells of very high aspect ratios is the only way acceptable. On this point structured mesh methods has the privileges to construct this kind of mesh with very high aspect ratio. Hence construction of unstructured grids combined with suitable elements distribution in the boundary layer region and the development of flow solution algorithms capable of producing accurate results is the subject of application of unstructured grids on viscous flow simulation . Some relevant researches have been reported recently [3][4][5][6]. Of these, a structured mesh, embedded within a globally unstructured mesh, has been utilised in the vicinity of the near-wall boundary layer to primarily ease the implemention of the turbulence model.

Here we propose a strategy, called the "SKIN" method, to construct the hybrid mesh with structured mesh in the near-wall regions and unstructured mesh in the other space. This application results in mesh which consists of an assembly of triangular and quadrilateral elements. The Euler flow solver has been used to do the validation. The code is a cell-centered, finite volume upwinding method with a point-Gauss-Seidel implicit time-stepping schemes. It can be used on mixed structured-unstructured quadrilateral-triangle meshes. Numerical tests have been made on different type of meshes, ie. unstructured mesh, structured mesh and hybrid mesh. The results show the flow code is efficient and robust on different meshes. The next step is to validate this type of hybrid mesh for viscous flow cases.

2. Grid Generation

2.1 Unstructured Grids

Several methodes have been developed to generate the unstructured meshes. Many have proved to be flexible for complex geometrical domains and for mesh adaption. Here use has been made of the advancing front technique (AFT) first developted by Peraire et al [7]. The process of AFT method is iterative: a front initialized by the set of given edges (ie. those describing the boundary and the specified line) , is analysed to determine a departure zone, from which one or several internal elements are created; the front is then updated and the element creation process is continued until the front is empty. Figure 2.1, adapted from ref.[8], shows the sample steps of the AFT method in 2-D. Let us consider the initial front that encloses the domain with the vertices 1-6 in Fig.2.1. The list of six front edges is shown at the right hand side. Note that these edges are not in any particuliar order but the orientation of the edge is unique, which means that along the edge from the first vertex to the second the domain is always on the left. The set of front edges is shown in thick lines. The thin line defines the constructed mesh. In step 2,3 two new vertices 7,8 have been created with four new edges 3-7, 7-4, 5-8, 8-6. Edges 3-4 and 5-6 have been removed. In step 4 edge 2-6 has been connected to the existing vertex 7 and two new edges 2-7, 7-6 have been created. Step 5 connects to edge 5-1 to the existing vertex 8 and only one new edge 8-1 is created, but two edges 5-1, 8-5 are removed. In step 6 the three edges 7-6, 6-8, 8-7 collapse, leading to a domain of two separate holes to be triangulated. In step 8 the process terminates as the list of frontal edges are exhausted. Figure 2.2 gives the unstructured mesh around the NACA 0012 airfoil using the AFT method.

2.2 Structured Grids

The popular approach for the generation of structured grids is based on the use of the algebraic interpolation method and partial differential equation solution. For simple configurations, such as an aerofoil, it is possible to map a single set of computational coordinates to curvilinear coordinates in the physical space.

The first structured grid generator used here is named ALGEM [9], a code using an algebraic multisurface interpolation method to generate a C-mesh around a streamlined body. For the domain shown in Fig.2.3, the boundary surface consists of a symmetric slender body extended downstream, ABC, and a farfield boundary, FED. Between these two half boundaries a C-mesh is to be generated. Because of the symmetry the complete C-mesh can finally be obtained by reflection about the x-axis. Grid generation is completed in two steps. First the distributed

boundary grid points are determined using one-dimensional stretching functions. Then the interior grid is generated by the multisurface technique. In the present code only two intermediate surfaces, each adjacent to the boundary ABC and FED, are introduced to guarantee the orthogonality. Finally the grid distribution is obtained by interpolation. Fig. 2.4 gives the C-mesh around the NACA 0012 airfoil using this method.

The second structured grid generator used is the EAGLE package, a general three-dimensional elliptic grid generation system developed by Thompson et al [10]. Mesh generation follows two steps. First generate the boundary points distribution. The second is the grid generation. Fig. 2.5 gives the C-mesh around the NACA 0012 aerofoil using the EAGLE package.

2.3 Hybrid Grids

At the present stage of development the contruction of an unstructured grid for viscous flow simulation still remains a challenge. The popular grid generation approaches of the Delaunay and advancing front, by their nature, do not lend themselves for the generation of the highly stretched elements required within a boundary layer of a viscous flow. Alternative technique need be investigated. In Ref.[1] three categories of approaches to viscous mesh construction are reviewed. The first technique[11] is to construct an equivalent structured grid close to the wall while using a standard unstructured grid generation procedure outside. The second [12] is to modify a generated regular grid by element transformation. The third[13] is to utilize an intermediate mapping space. Reference[14] reviews some recent progress [3][4][5][6] and also gives the details about two interesting and efficient methods, namely Node Attraction and Advancing Normals, designed to construct the viscous mesh based on the unstructured mesh. Here we propose a simple and efficient strategy, called the "SKIN" method, to construct the hybrid mesh based on both structured and unstructured mesh geneartors. The method is based on the division of the flow domain into two regions, one near the solid wall and the other off the wall. The structured mesh is generated within the inner region and the unstructured mesh is generated in the outer region. Two types of mesh are mixed in the interface. The basic steps are outlined below.

Step 1: Define the geometry of body considered;

Step 2: Generate the structured mesh around that body (e.g. using ALGEM code or EAGLE package);

Step 3: Pick one grid line around that body as a virtual boundary line, resulting in a virtual body shape. It looks like a "skin" attached to the real body;

Step 4: Generate an unstructured mesh beyond the virtual body and domain;

Step 5: Check the compatibility of the two grids at the interface between the outer unstructured and the inner structured grids. If incompatible refine or coarsen the inner structured mesh points;

Step 6: Combine the outer region unstructured mesh and the inner region structured mesh into a hybrid mesh.

Fig. 2.6 gives the procedure for the use of the "SKIN" method applied to an aerofoil shape.

2.4 A general grid approach

Fig.2.7 gives a schematic of the interconnections between different grid types, flow solver and adaptive remeshing.

3. Adaptivity[15]

To catch the features of a flowfield accurately, it is necessary to introduce grid adaptivity techniques. Adaptivity is based on the equidistribution principle

$$w_i ds_i = \text{constant} \qquad (3.1)$$

where w_i is the error or activity indicator at node i and ds_i is the local grid point spacing at node i. This principle can be satisfied by the use of different methods, including point enrichment, point derefinement, node movement and remeshing, or any combination of them. In this paper we adopt the remeshing procedure to implement the adaptivity.

After computation on an initial mesh the result is examined to determined those elements in which large flow gradients are present. The analysis performed is

(1) for each edge determine

$$\varphi_{ave} = 0.5(\varphi_e + \varphi_r) \qquad (3.2)$$

where φ refers to the flow variables chosen to be an indicator of gradients and subscripts e,r represent the two elements connecting the same edge;

(2) Test the deviation of φ_i away from the mean value, ie.

$$\Gamma_i = \frac{|\varphi_{ave} - \varphi_i|}{\varphi_{ave}} \qquad (3.3)$$

(3) if $\Gamma_i \geq \Phi$, where Φ is the deviator factor. Φ=0.05-0.2

Then this edge must be in a region of large gradient.

After analysis the assemlly of all edges in the large gradient region is then found. Some control parameter is then changed and the remeshing procedure follows.

Another very simple method to identify the high gradient region ,e.g. shock wave region, can be performed by checking the solution contours. After computation on the initial mesh the flow

results and the grid data can be used to generate contour plots. From the plots we can find the regions of dense contour line signed the high gradients. Smaller elements are needed in that region and so a remeshing procedure can be implemented as above.

4. Euler Flow Solver

4.1 The governing equations

The flow of an ideal, inviscid, compressible fluid is governed by the Euler equations. They represent the conservation of mass, momentum and energy. For 2D flow, the integral form of the equations can be written as

$$\int_{\Omega_e} \frac{\partial U}{\partial t} d\Omega = \int_{\Gamma_e} -n_i F_i d\Gamma \qquad i = 1,2 \qquad (4.1)$$

Where: $n_i = (n_1, n_2)$ denotes the unit vector outward normal to the boundary Γ_e of the control volume Ω_e. and the integrals are taken over a contral volume Ω_e, bounded by the curve Γ_e . The conserved variables and the Cartesian flux functions are given by

$$U = \begin{pmatrix} \rho \\ \rho u \\ \rho v \\ \rho \varepsilon \end{pmatrix} \qquad F_1 = \begin{pmatrix} \rho u \\ \rho u^2 + P \\ \rho uv \\ u(\rho \varepsilon + P) \end{pmatrix} \qquad F_2 = \begin{pmatrix} \rho v \\ \rho vu \\ \rho v^2 + P \\ v(\rho \varepsilon + P) \end{pmatrix} \qquad (4.2)$$

where ρ is the density, u,v are the Cartesian velocity components, p is the pressure, ε is the total internal energy per unit volume. The temperature T is obtained from the equation of state which closes the system

$$p = (\gamma - 1)\rho T \qquad (4.3)$$

where γ is the ratio of specific heats.

The boundary conditions for the Euler equations at solid surfaces are that of no normal flow. A one-dimensional characteristic analysis is used to deal with the boundary conditions at the far-field.

4.2 Numerical algorithm - PGS scheme

For a cell-centered scheme, assuming a piecewise constant distribution of the unknowns U_e on each element Ω_e , Eq(4.1) may be approximated in the form as

$$\Delta U_e = U_e^{n+1} - U_e^n = \frac{\Delta t_e}{\Omega_e} F^I \qquad (4.4)$$

Where: U_e^n denotes the valus of U_e at time $t = t^n$, $\Delta t = t^{n+1} - t^n$ is the time step between t^{n+1} and t^n , F^I denotes the inviscid contribution.

The inviscid contributions F^I are given by

$$F^I = \int_{\Gamma_e} -n_i F_i d\Gamma = -\int_{\Gamma_e} F_n d\Gamma \tag{4.5}$$

and can be evaluated by summing the contributions from each individual element side Γ_{es} in turn. In this evaluation the normal flux F_n is replaced by a numerical flux $\tilde{F}_n$, so that

$$F^I = -\sum_{Se} \int_{\Gamma_{es}} \tilde{F}_n d\Gamma \tag{4.6}$$

For a typical side Γ_{es} with associated elements e and r, Roe's linearization is used to construct the matrix A_{roe}, such that

$$F_{nr} - F_{ne} = A_{roe}(U_r - U_e) \tag{4.7}$$

and the numerical flux is then taken to be

$$\tilde{F}_n = 0.5[F_{ne} + F_{nr} - |A_{roe}|(U_r - U_e)] \tag{4.8}$$

Here it has been assumed that A_{roe} has been factored as

$$A_{roe} = R^{-1}\Lambda R \tag{4.9}$$

where Λ is a diagonal matrix containing the eigenvalues λ_i of A_{roe} and $|A_{roe}|$ is defined by

$$|A_{roe}| = R^{-1}|\Lambda|R \tag{4.10}$$

The mininum allowable value for λ_i must be restricted and is such that:

$$|\lambda_i| = \begin{cases} |\lambda_i| & |\lambda_i| > \varepsilon_\lambda \\ 0.5(\lambda_i^2 / \varepsilon_\lambda + \varepsilon_\lambda) & |\lambda_i| \le \varepsilon_\lambda \end{cases} \tag{4.11}$$

where ε_λ is the eigenvalue limiter.

If the inviscid contributions are evaluated at time t^{n+1}, equation (4.4) leads to the implicit scheme

$$\Delta U_e = -\frac{\Delta t_e}{\Omega_e} \sum_{S_e} \left\{ \frac{1}{2}\left[F_e^{n+1} + F_r^{n+1} - |A_{Roe}^{n+1}|(U_r^{n+1} - U_e^{n+1}) \right] \right\} \delta s_e \tag{4.12}$$

Linearization of this equation for the values of the unknowns and fluxes result in

$$\left[I + \frac{\Delta t_e}{2\Omega_e} \sum_{S_e} |A_{Roe}^*| \delta s_e \right] \Delta U_e^{n+1} = -\frac{\Delta t_e}{2\Omega_e} \sum_{S_e} \left[F_e^n + F_r^* - |A_{Roe}^*|(U_r^* - U_e^n) \right] \delta s_e \tag{4.13}$$

where the linearization has been performed with an iterative solution in mind and the terms denoted by an asterisk are evaluted using the latest available solution in the adjacent elements. Thus the iterative procedure may be regarded as a point-Gauss-Seidel method requiring the inversion of a 4*4 matrix for each element in the computational grid. High order resolution is also achieved [16].

5. Results and discussions

To demonstrate the application of the method presented, inviscid transonic flow around the aerofoil is considered. The result illustrate the flow solver on an unstructured mesh, a structured mesh and a hybrid mesh, respectively.

5.1 Unstructured mesh

The unstructured mesh around airfoil is generated by the AFT method. The first test case is NACA0012 airfoil in a free stream flow of Mach number 0.75. The incidence is 2.0 deg. Fig.5.1 gives the Mach number contours on an initial mesh (Mesh1: 3246 elements and 1670 nodes), fine mesh (Mesh2: 6354 elenments and 3267 nodes) and adaptive mesh (Mesh3: 8558 elements and 4381 nodes), respectively. It can be seen that after adaption the shoch wave can be captured accurately. Fig.5.2 illustrates the results of the unstructured mesh topology and the Mach number contours in the test case at Mach number 0.80 and angle of attack of 1.25 degree. A well simulated result has also been achieved after the adaption remeshing procedure. The third test case is the supercritical airfoil RAE 2822 at a Mach number of 0.75 and angle of attack of 3.0 degree. Fig.5.3 gives the mesh and the Mach number and pressure contours. All the above simulations have been done using the Euler solver code described in Section 4.

5.2 Structured mesh

The first structured mesh generator used is ALGEM [9]. It can generate a C-mesh around a body using a multisurface algebraic method. Fig.5.4 presents the computational results (the Mach number is 0.75 and incidence is 2.0 degrees) on: a structured mesh (101×51 grid points); a regular unstructured mesh (10000 elements, 5151 nodes); and a regular-staggered unstructured mesh (10000 elements, 5151 nodes), respectively. As there are only 60 points around the airfoil (30 points on upper surface and 30 points on lower surface), it can be seen from the Mach number contours that the shock wave can be captured but it is not very well resolved. The pressure distribution on the surface (see Fig.5.5) also illustrates this deficiency. Fig.5.6 illustrates some initial tests of the hybrid mesh method. The mesh, here we call it a Mixed mesh, is formed very simply by keeping the inner region as a structured mesh (here we use a 10 layer region) and changing the outer region mesh type to either a regular unstructured mesh or a regular-staggered unstructured mesh. Fig.5.6 illustrates the mesh topology and the corresponding pressure contours. Fig.5.7 makes a comparison of the pressure coefficients calculated on the structured mesh and the other two types of Mixed meshes.

The second structured mesh generator here used is the well-known EAGLE package[10]. The test case considered is a free stream flow of Mach number 0.80 with the aerofoil at zero angle of attack. Fig.5.8 shows the comparison of the pressure contour on a structured mesh

(161×33 grid points), a regular unstructured mesh (10240 elements, 5313 nodes) and a regular-staggered unstructured mesh (10240 elements, 5313 nodes). Fig.5.9 provides a comparison of the respective C_P distributions. The Mixed mesh is again formed and the results are compared with those obtained on the structured mesh (Fig.5.10). Here a 5 layer region is retained as the structured mesh topology and the other mesh region is changed into a regular unstructured mesh or a regular-staggered unstructured mesh. The total elements are 9440. Fig.5.11 provides a comparison of the respective surface pressure distributions which show good agreement between the various meshes.

5.3 Hybrid mesh

The proposed "SKIN" method is used to generate the hybrid mesh around body. As illustrated in Section 2.3 first the structured mesh is generated around the body. One of mesh lines is selected as the virtual body boundary and the unstructured mesh is generated in the outside region by the AFT method. The final step is to combine the two types of mesh into a hybrid mesh. The computations are compared in Fig.5.12 (the test case is Mach number 0.75 with an angle of attack of 2 degree) on an unstructured mesh (3246 elements and 1670 nodes), a hybrid mesh (with a 9 layer structured mesh topology this results in a total of 4757 elements and 3045 nodes) and an adaptive hybrid mesh (with a 9 layer structured mesh topology but with a refined mesh in the adaptive region results in a total of 5507 elements and 3303 nodes), respectively. It can be seen that the contour lines are not very smooth at the junction between the inner structured and outer unstructured meshes. This may arise for the reason that the mesh spacing is not very smooth in that zone. In the present "SKIN" method a mesh smoothing technique has not yet been considered. The results will be expected to be improved after using the more smooth mesh topology. Fig.5.13 shows the comparison of the C_P distribution. Another test case on the hybrid mesh is at a Mach number of 0.8 with a 1.25 degree angle of attack. Fig.5.14 shows the resulted mesh and pressure contours. Unsmooth features can also be seen at the interface between the unstructured and structured meshes, the expected reason being the same as discussed above. Fig.5.15 shows the respective comparison of pressure coefficient. In both hybrid meshes the inner structured mesh topology is adapted from the ALGEM code. The following hybrid mesh is generated by using the EAGLE package to construct the inner region of the structured mesh, regular unstructured mesh and regular-staggered unstructured mesh, respectively while the outer region of the unstructured mesh is generated by the AFT method. The comparison has been made using the test case of Mach number 0.80, angle of attack 1.25° (see Fig.5.16) Here 4 layers are chosen for the inner region with the resulting in a mesh size change between inner region and outer region which is very small. This results in improved pressure contours. No obvious lack of smoothness appears. Fig.5.17 illustrates the comparison of pressure coefficient distribution between the unstructured mesh and the three kinds of hybrid meshes.

6. Conclusions

Methods of mesh generation have been discussed. A cell-centered, finite volume Euler flow solver has been demonstrated on unstructured and structured meshes. One strategy, called the "SKIN" method, is proposed to construct the hybrid mesh. The improved Euler flow solver is also validated on the resultant hybrid mesh. Results demonstrate the good quality of this hybrid mesh. It has the potential to be used in viscous flow simulation in future.

Acknowledgement

The author wishes to thank Dr.X.Xu for the discussion on some ideas of the hybrid method.

References

[1] J.F.Thompson, N.P.Weatherill "Aspects of Numerical Grid Generation: Current Science and Art" AIAA-Invited Paper 11th AIAA Applied Aerodynamics Conference, Aug 9-11,1993

[2] N.P.Weatherill "Mixed Structured-Unstructured Meshes for Aerodynamics Flow Simulation" Aeronautical J. Apr.1990, pp111-123

[3] F.Chalot, J.Zdenek, M.Mallet, M.Ravachol and G.Roge "Development of a Finite Element Navier-Stokes Solver with Applications to Turbulent and Hypersonic Flows" AIAA 92-0670,1992

[4] D.L.Marcum and R.K.Agarwal " A Finite Element Navier-Stokes Solver for Unstructured Grids " AIAA J. Vol.30, p648,1992

[5] K.Nakahashi " Adaptive Prismatic Grid Method for External Viscous Flow Computations " AIAA paper 93-3314,1993

[6] D.J.Mavriplis " Algebraic Turbulence Modelling for Unstructured and Adaptive Meshes " AIAA J. Vol. 29 No.12 pp2086,1992

[7] J.Peraire, M.Vahdati, K.Morgan and O.C.Zienkiewicz "Adaptive Remeshing for Compressible Flow Computations " J. Comp. Phys. 72, 449-466, 1987

[8] J.D.Muller " The Advancing Front Method and The Delaunay Triangulation " Lecture Series 1994-02, von Karman Institute for Fluid Dynamics Jan.24-28,1994

[9] C.A.J.Fletcher " Computational Techniques for Fluid Dynamics " Vol.II Chap.13

[10] J.F.Thompson, L.E.Lijewski, J.Cipolla and B.Gatlin "Program EAGLE User's Manual" Vol.I - Introduction and Grid Applications AFATL-TR-88-117, 1988

[11] Mavriplis D.J. " Algebraic Turbulence Modelling for Unstrctured and Adaptive Meshes " AIAA-90-1653

[12] Pirzadeh S. " Unstructured Viscous Grid Generation by Radvanary Front Method " 11th AIAA Applied Aerodynamics Meeting: Monterey,USA Aug.9-11,1993

[13] Holmes,G. and S.D. Connell " Solution of the 2D Navier-Stokes Equations on Unstrctured Adaptive Grids " AIAA-89-1932CP

[14] N.P.Weatherill, O.Hassan, D.L.Marcum, M.J.Marchant " Grid Generation by the Delaunay Triangulation " Lecture Series 1994-02, von Karman Institute for Fluid Dynamics Jan.24-28,1994

[15]Y.F.Yao " Simulation of Compressible Inviscid Flow on Adaptive Remeshing Unstructured Meshes " Dept. of Aerospace Engineering Aero. report 9424 Nov.15, 1994

[16]Y.F.Yao " Implicit High-Order Resolution of Supersonic Flow on Unstructured Meshes " Dept. of Aerospace Engineering Aero. report 9405 May 31, 1994

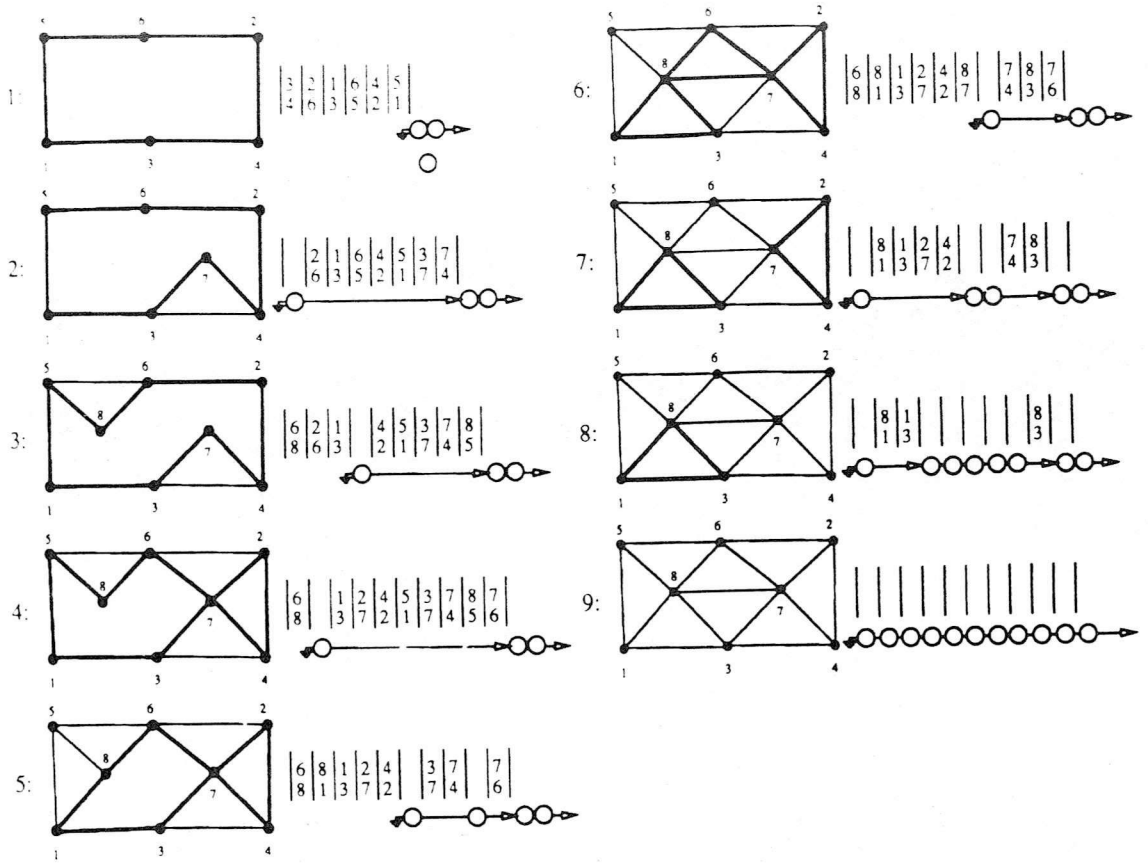

Fig. 2.1 Sample steps of the AFT method in 2-D. The front is given as the list of edges between the vertices on the right. Depicted below the list of frontal edges is the linked list that points to vacant storage in the front.

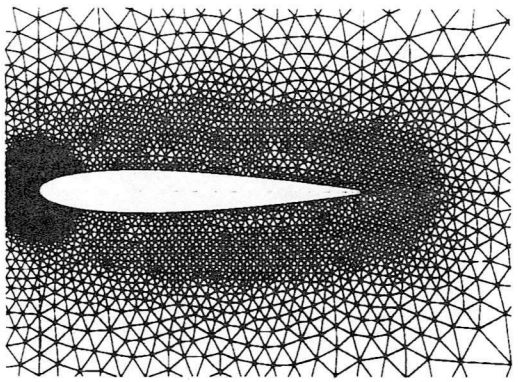

Fig.2.2 Unstructured mesh around NACA 0012 aerofoil using AFT method

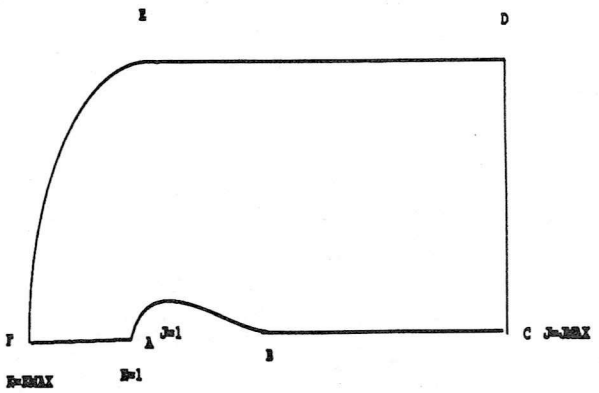

Fig.2.3 Computational domain for ALGEM code

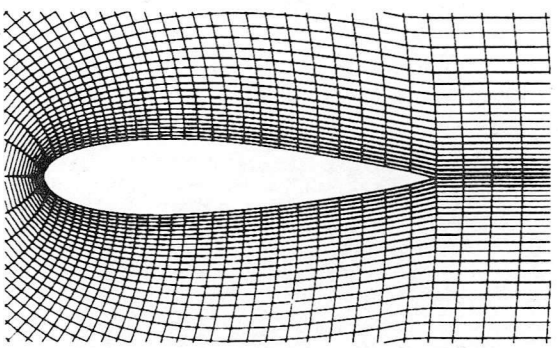

Fig.2.4 Structured mesh around NACA 0012 aerofoil using ALGEM code

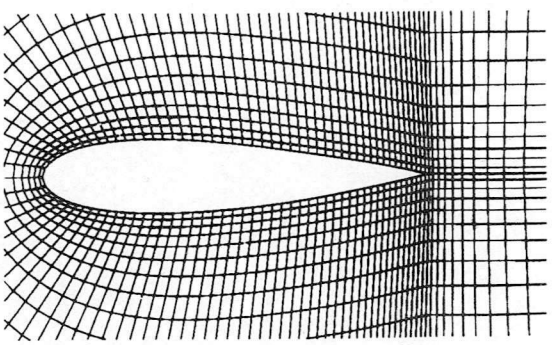

Fig.2.5 Structured mesh around NACA 0012 aerofoil using EAGLE package

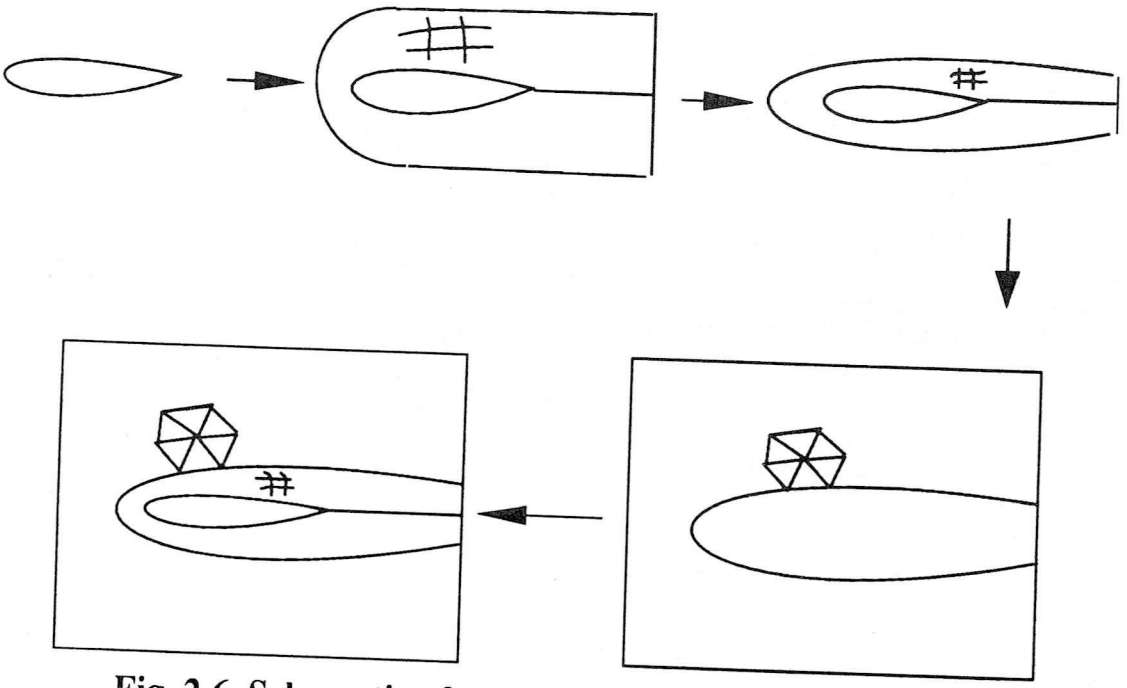

Fig. 2.6 Schematic of the "SKIN" method

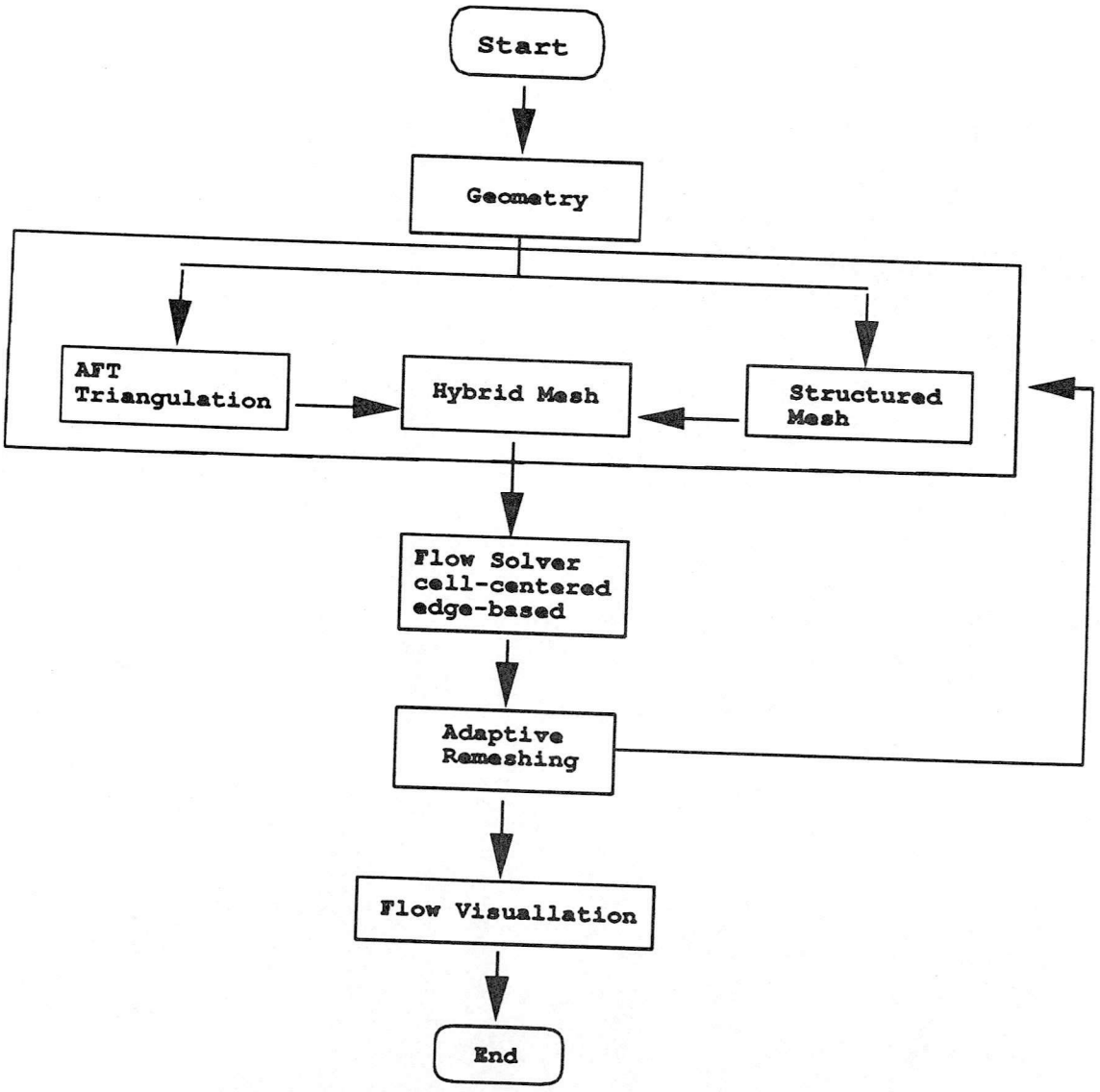

Fig. 2.7 Schematic of a generalised grid approach

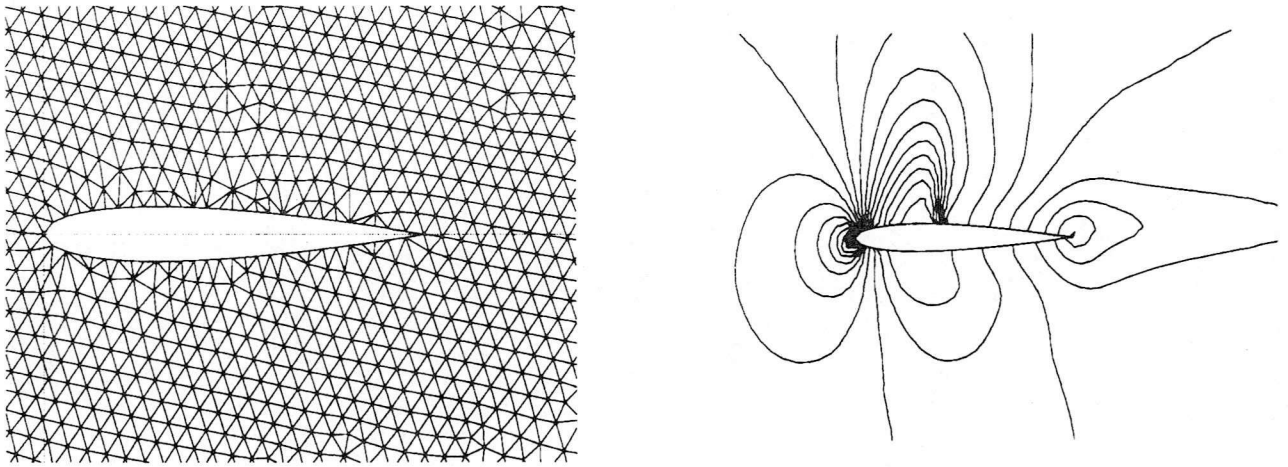

Fig.5.1(a) NACA 0012 Airfoil
Mesh 1: 3246 elements 1670 nodes
Mach number contour: Mach=0.75 Alp=2.0 Deg

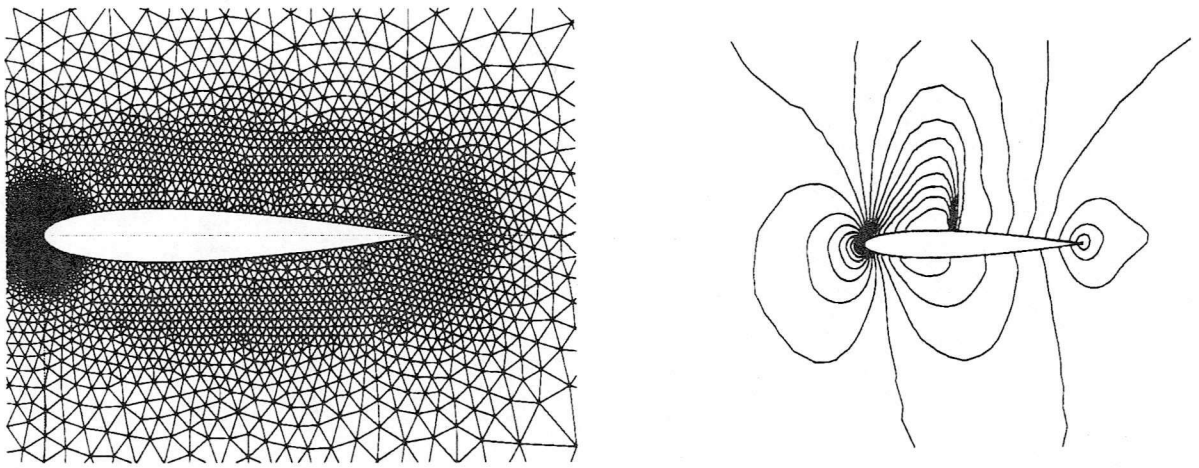

Fig.5.1(b) NACA 0012 Airfoil
Mesh 2: 6354 elements 3267 nodes
Mach number contour: Mach=0.75 Alp=2.0 Deg

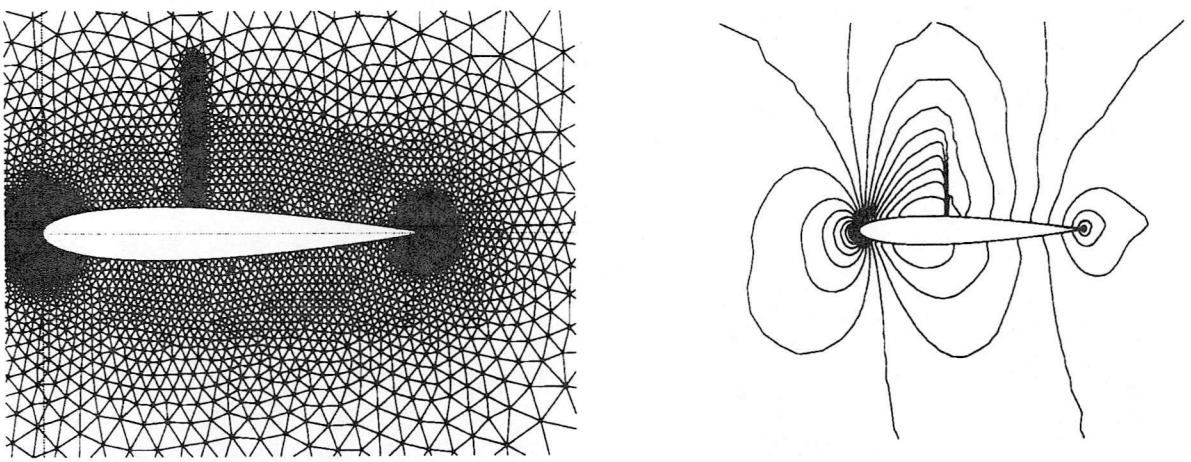

Fig.5.1(c) NACA 0012 Airfoil
Mesh 3: 8558 elements 4381 nodes
Mach number contour: Mach=0.75 Alp=2.0 Deg

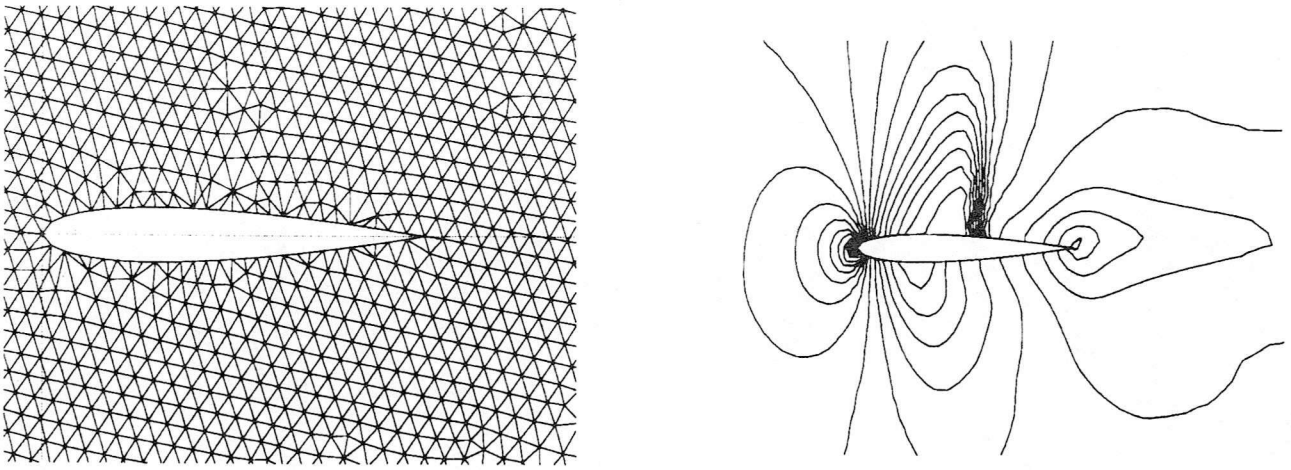

Fig.5.2(a) NACA 0012 Airfoil
Mesh 1: 3246 elements 1670 nodes
Mach number contour: Mach=0.80 Alp=1.25 Deg

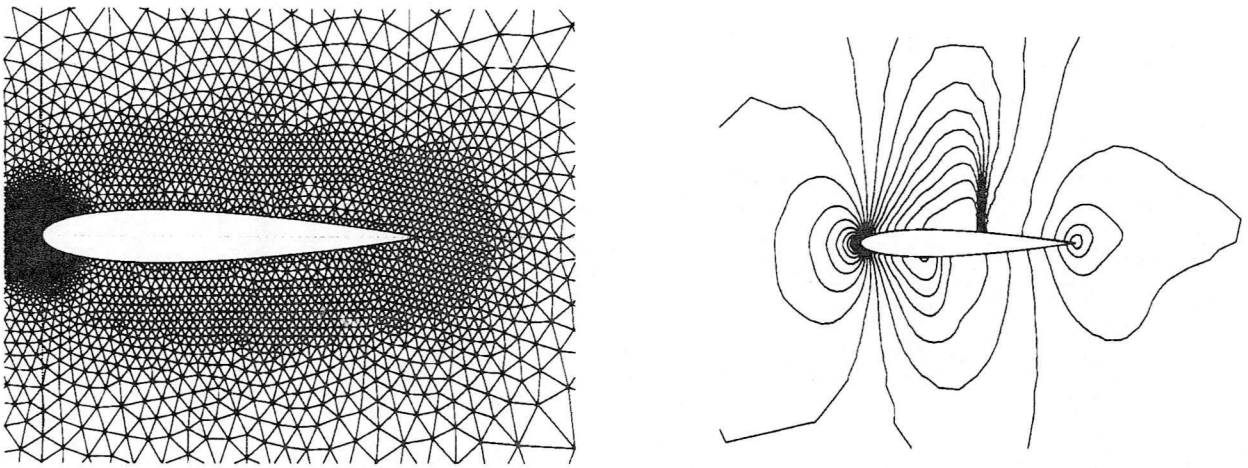

Fig.5.2(b) NACA 0012 Airfoil
Mesh 2: 6354 elements 3267 nodes
Mach number contour: Mach=0.80 Alp=1.25 Deg

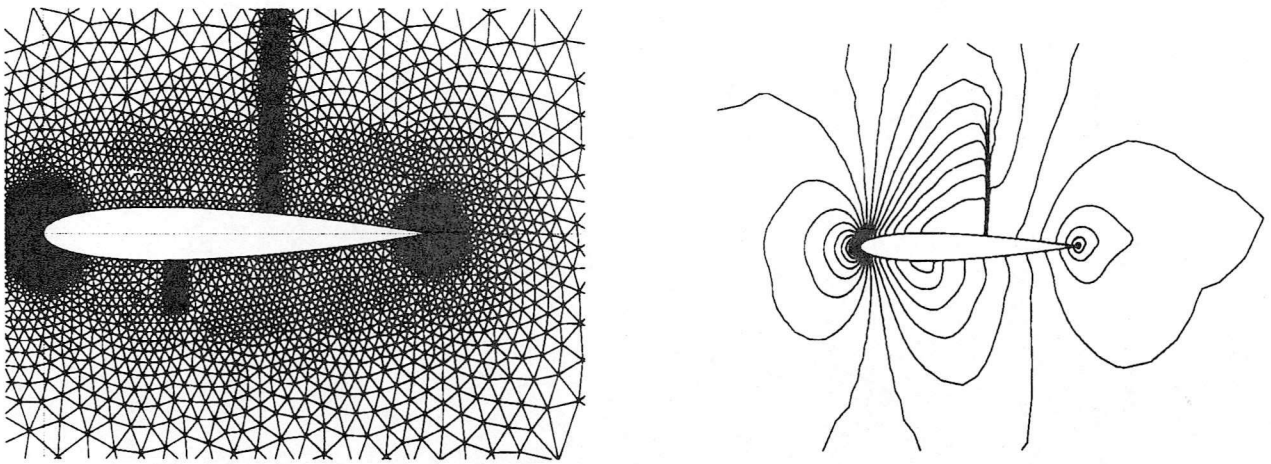

Fig.5.2(c) NACA 0012 Airfoil
Mesh 3: 9769 elements 4988 nodes
Mach number contour: Mach=0.80 Alp=1.25 Deg

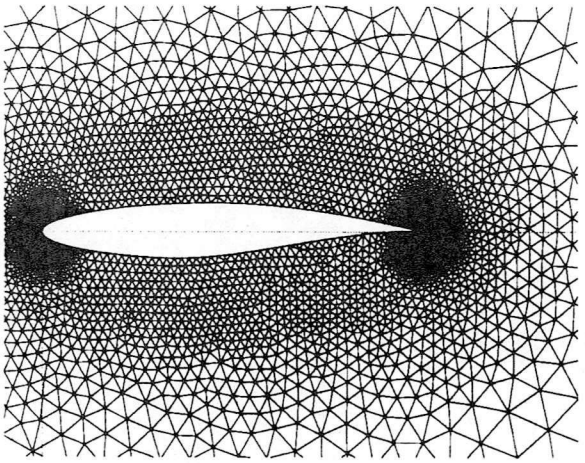

(a) Mesh1: 6674 elements
3426 nodes

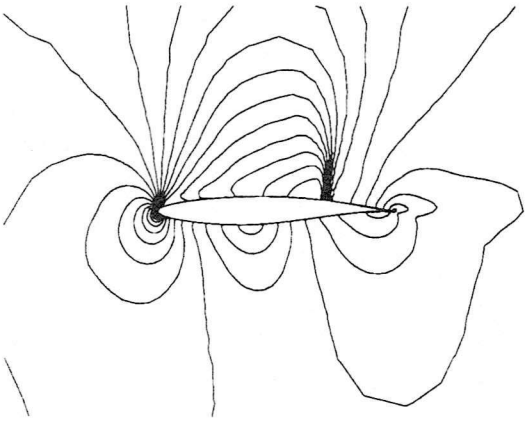

(b) Mach number contour

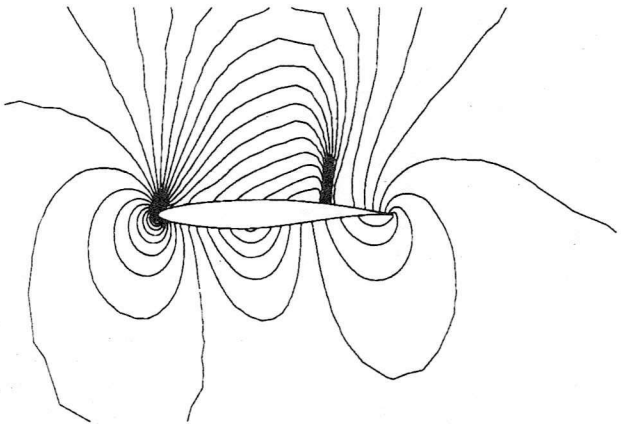

(c) Pressure contour

Fig.5.3.1 RAE 2822 Airfoil
Mach=0.75
Alp=3.0 Deg

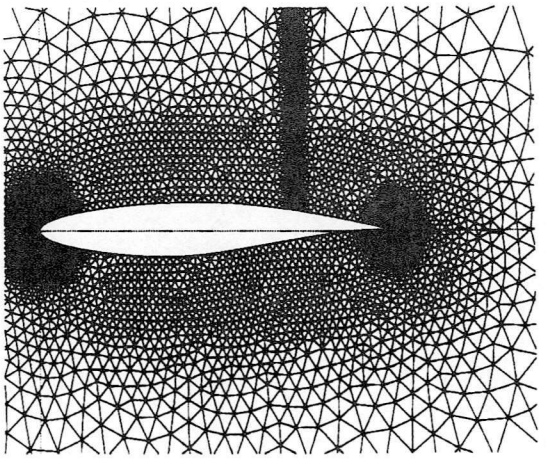

(a) Mesh2: 9506 elements
4850 nodes

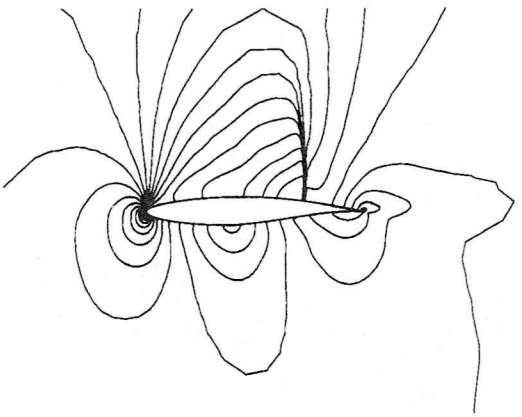

(b) Mach number contour

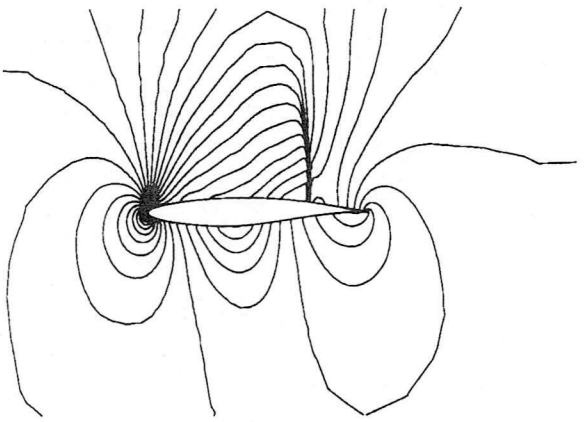

(c) Pressure contour

Fig.5.3.2 RAE 2822 Airfoil
Mach=0.75
Alp=3.0 Deg

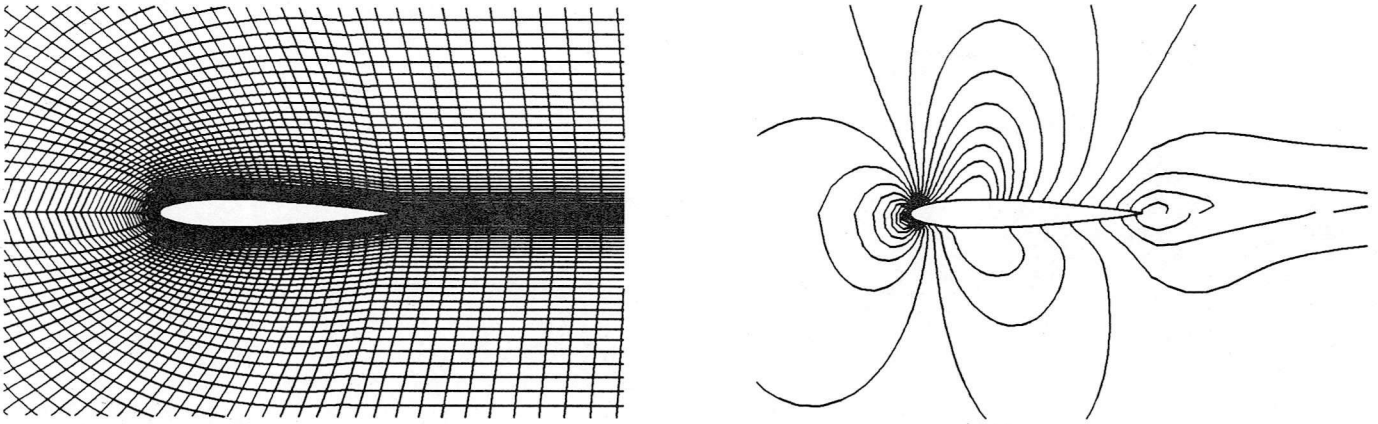

Fig.5.4(a) NACA 0012 airfoil Mesh generator: ALGEM code
Structured mesh: 5000 elements 5151 nodes
Mach number contour: Mach=0.75 Alp=2.0 deg

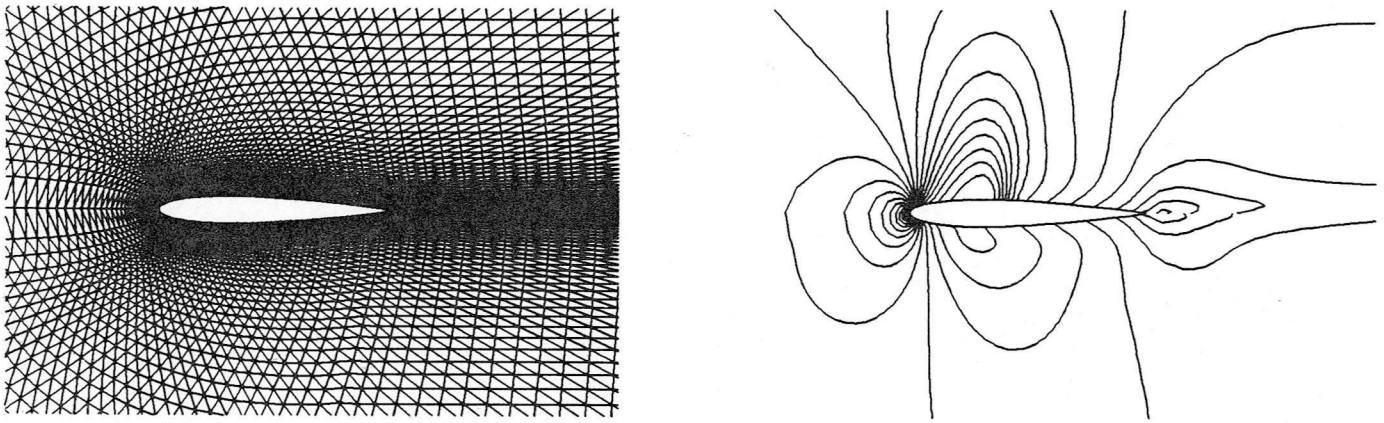

Fig.5.4(b) NACA 0012 airfoil Mesh generator: ALGEM code
Regular unstructured mesh: 10000 elements 5151 nodes
Mach number contour: Mach=0.75 Alp=2.0 deg

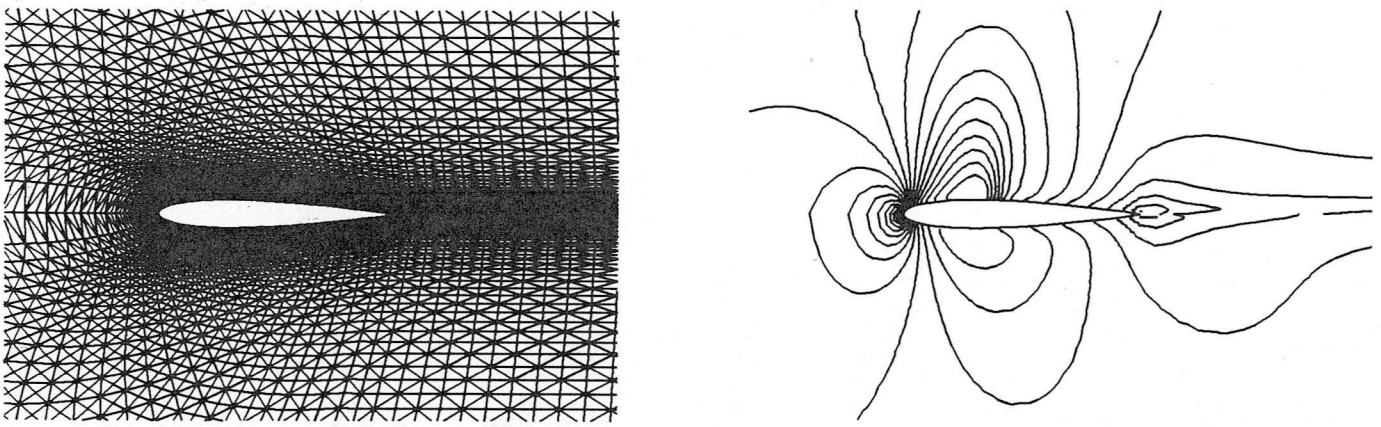

Fig.5.4(c) NACA 0012 airfoil Mesh generator: ALGEM code
Regular–staggered unstructured mesh: 10000 elements 5151 nodes
Mach number contour: Mach=0.75 Alp=2.0 deg

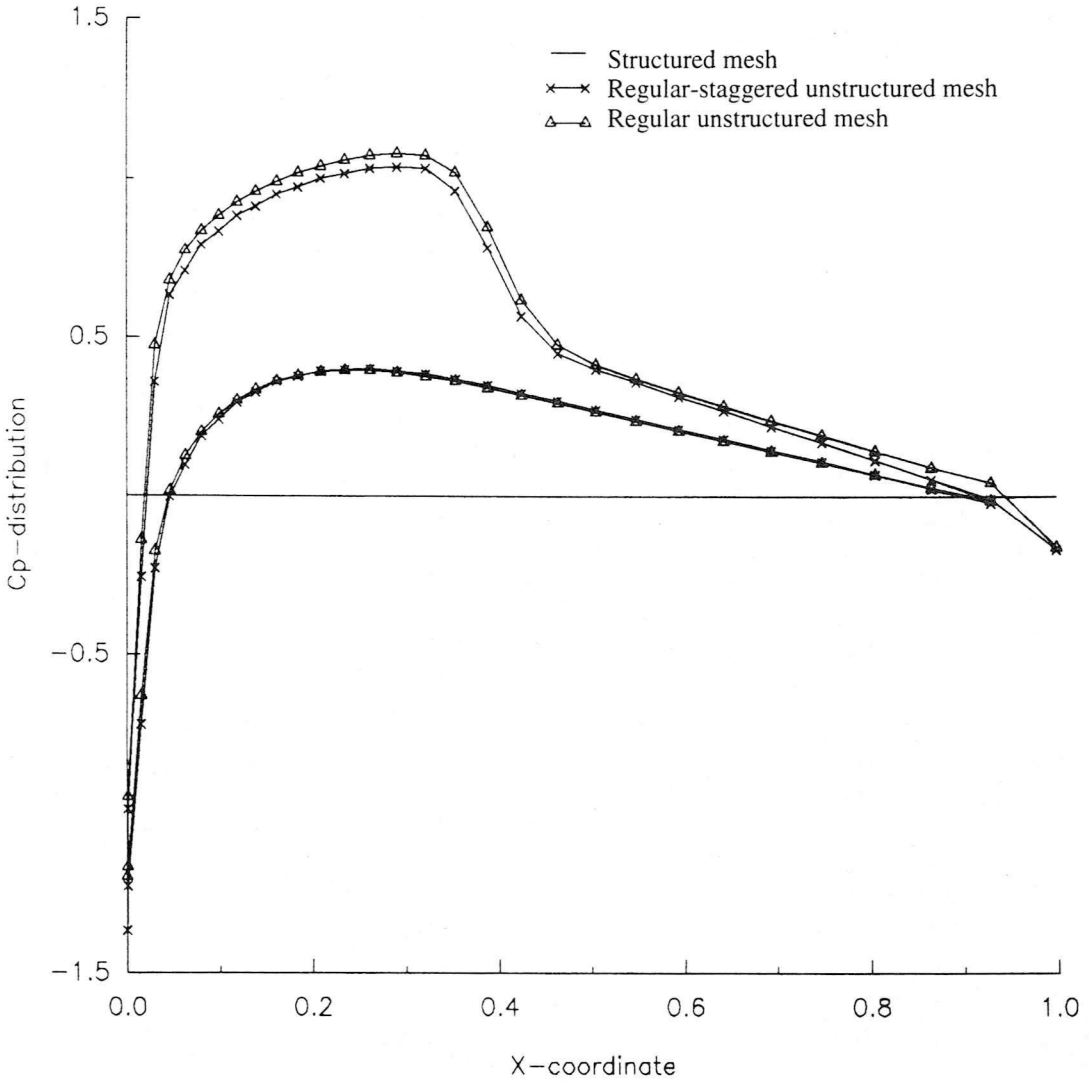

Fig. 5.5 Comparison of pressure coefficient on meshes generated by ALGEM code
Mach=0.75 Alp=2.0 deg.

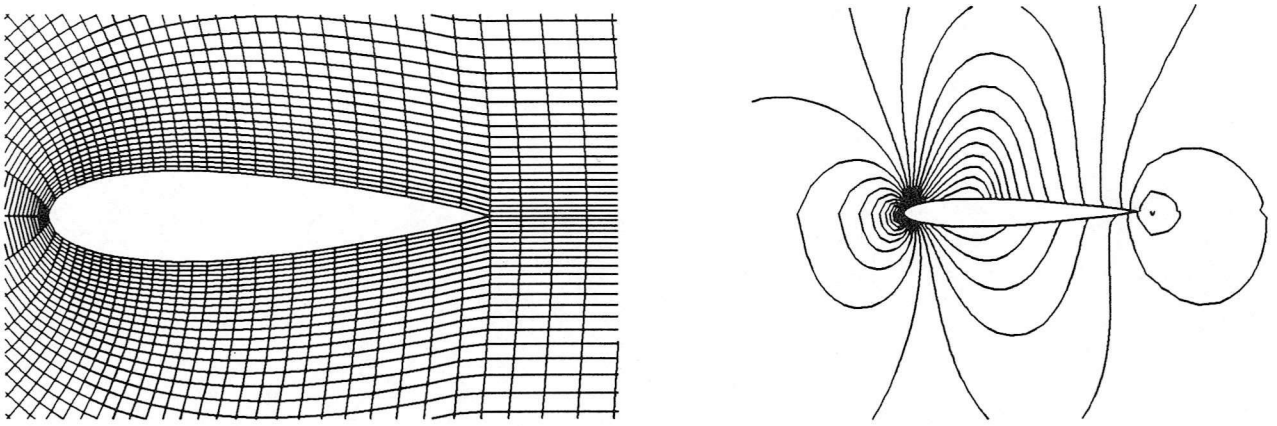

Fig.5.6(a) NACA 0012 airfoil Mesh generator: ALGEM code
Structured mesh: 5000 elements 5151 nodes
Pressure contour: Mach=0.75 Alp=2.0 deg

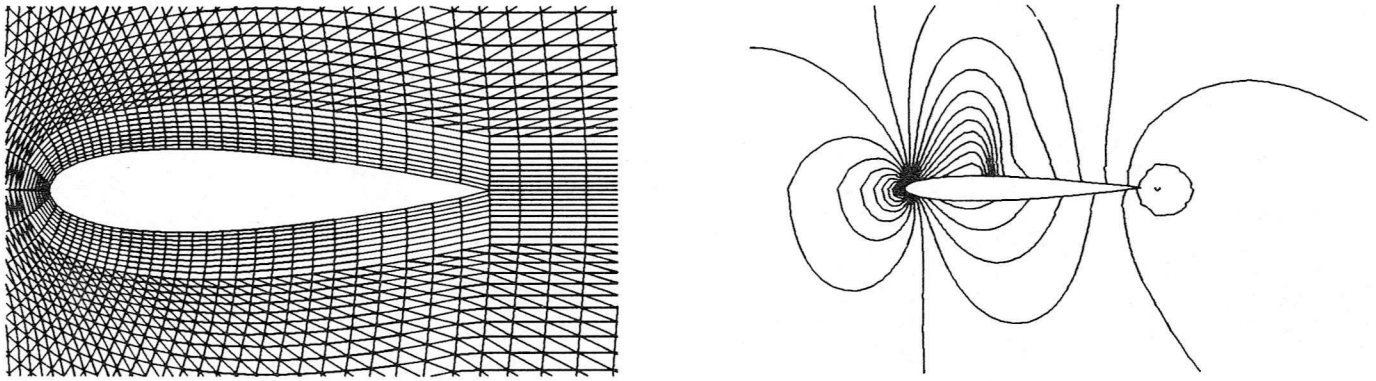

Fig.5.6(b) NACA 0012 airfoil Mesh generator: ALGEM code
Mixed mesh: inner region --- Structured mesh
outer region --- Regular unstructured mesh
total : 9100 elements 5151 nodes
Pressure contour: Mach=0.75 Alp=2.0 deg

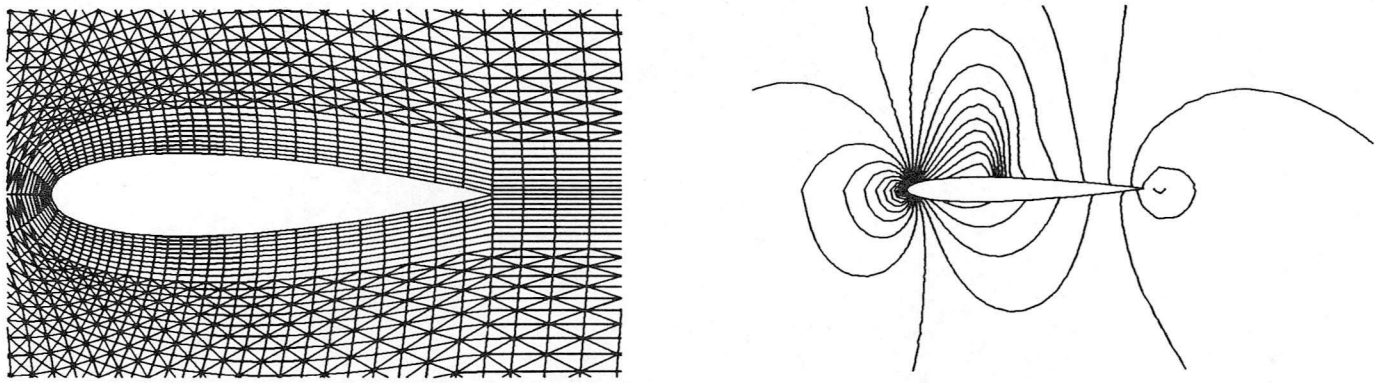

Fig.5.6(c) NACA 0012 airfoil Mesh generator: ALGEM code
Mixed mesh: inner region --- Structured mesh
outer region --- Regular-staggered unstructured mesh
total : 9100 elements 5151 nodes
Pressure contour: Mach=0.75 Alp=2.0 deg

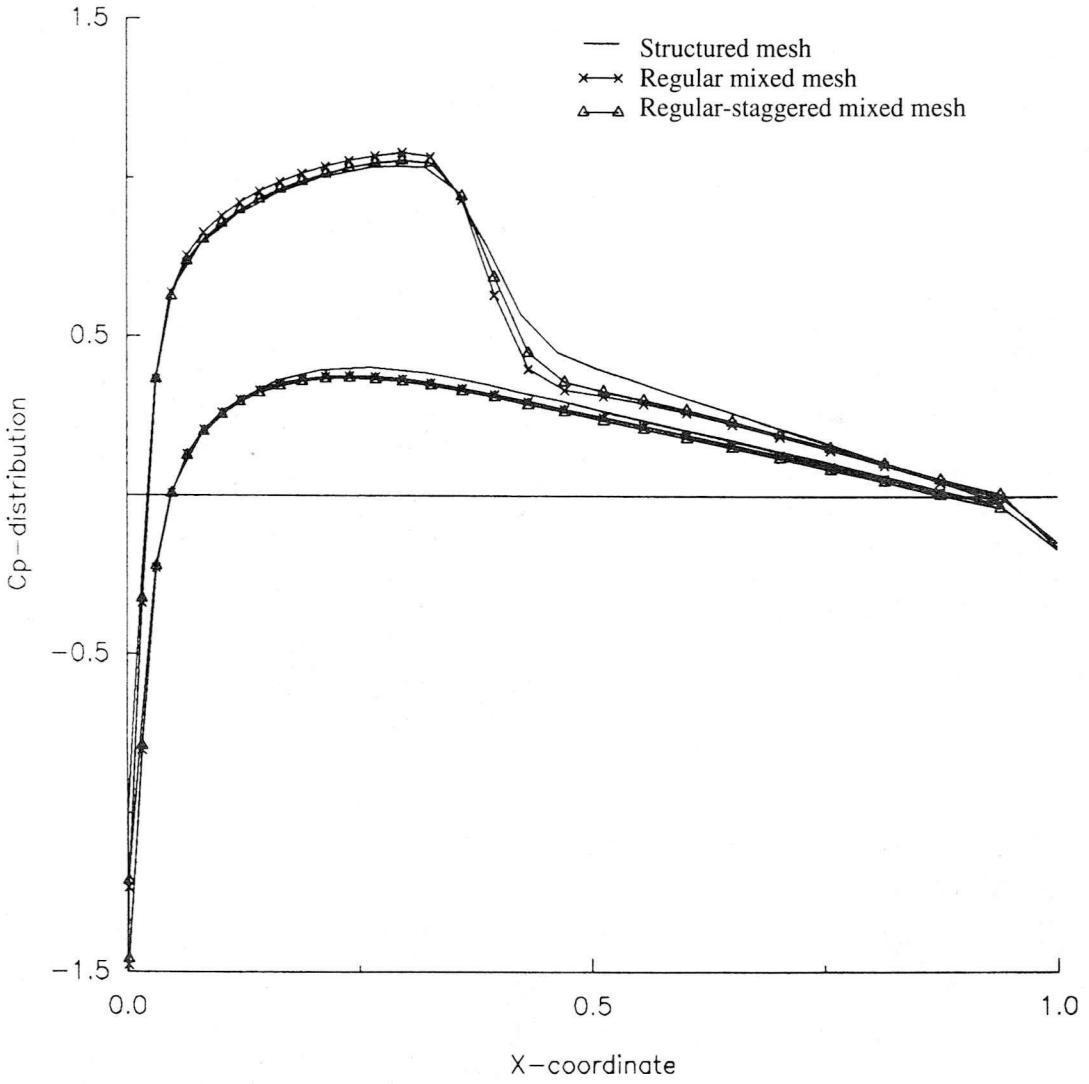

Fig. 5.7 Comparison of pressure coefficient on structured mesh and mixed meshes generated by ALGEM code
Mach=0.75 Alp=2.0 deg.

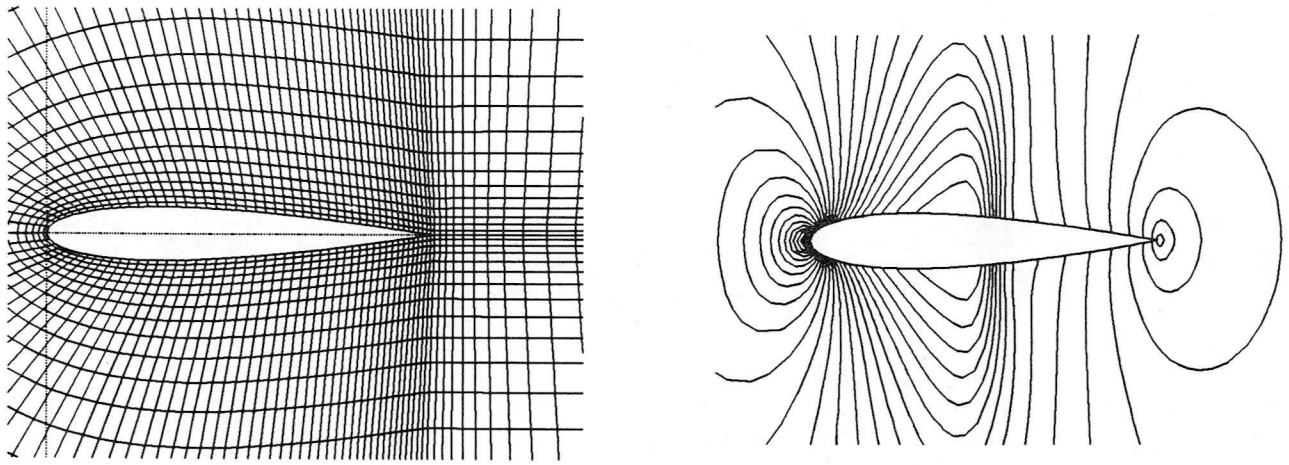

Fig.5.8(a) NACA 0012 airfoil Mesh generator: EAGLE package
Structured mesh: 5120 elements 5313 nodes
Pressure contour: Mach=0.80 Alp=0.0 deg

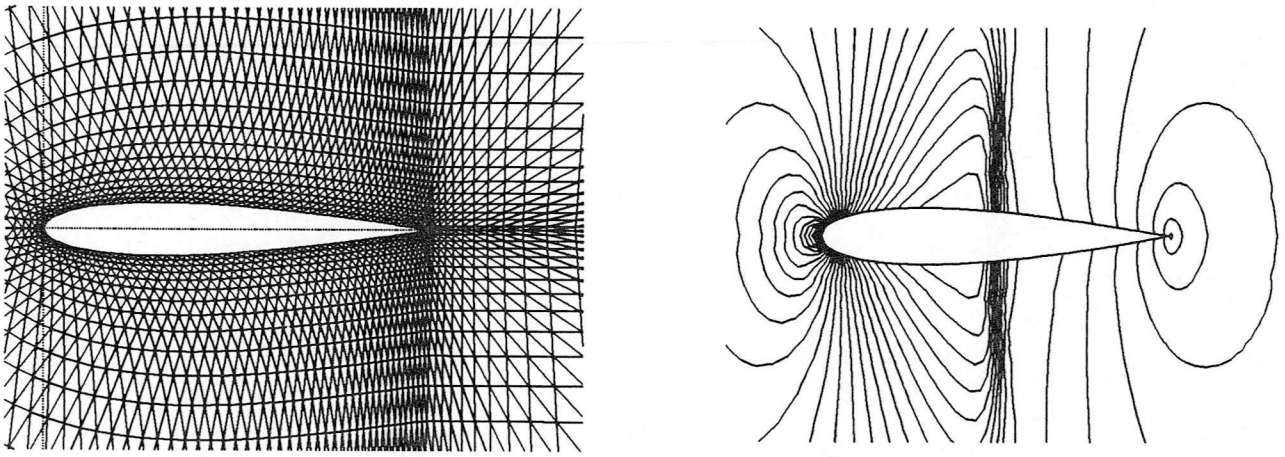

Fig.5.8(b) NACA 0012 airfoil Mesh generator: EAGLE package
Regular structured mesh: 10240 elements 5313 nodes
Pressure contour: Mach=0.80 Alp=0.0 deg

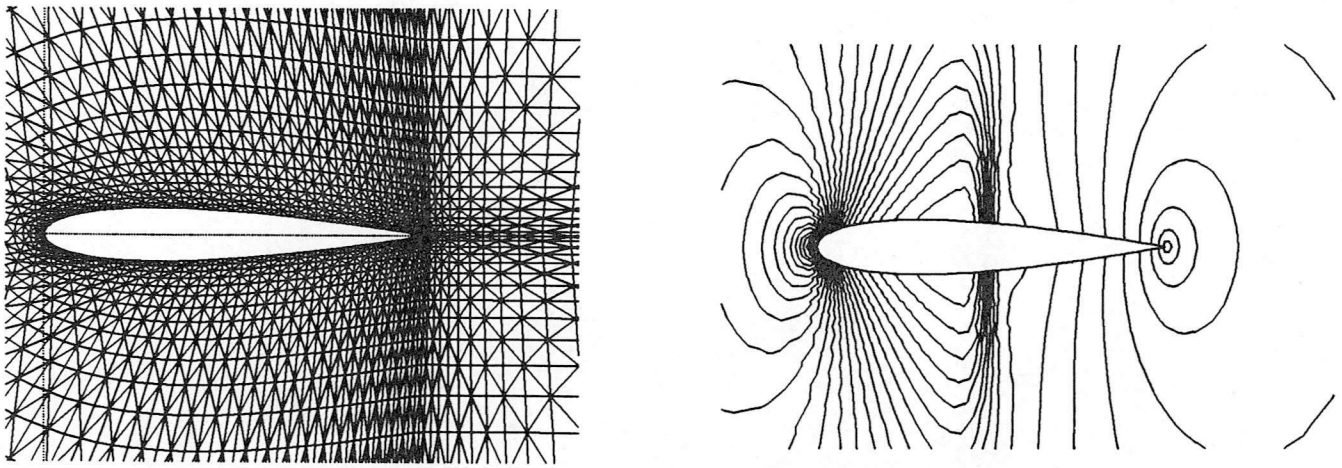

Fig.5.8(c) NACA 0012 airfoil Mesh generator: EAGLE package
Regular–staggered structured mesh: 10240 elements 5313 nodes
Pressure contour: Mach=0.80 Alp=0.0 deg

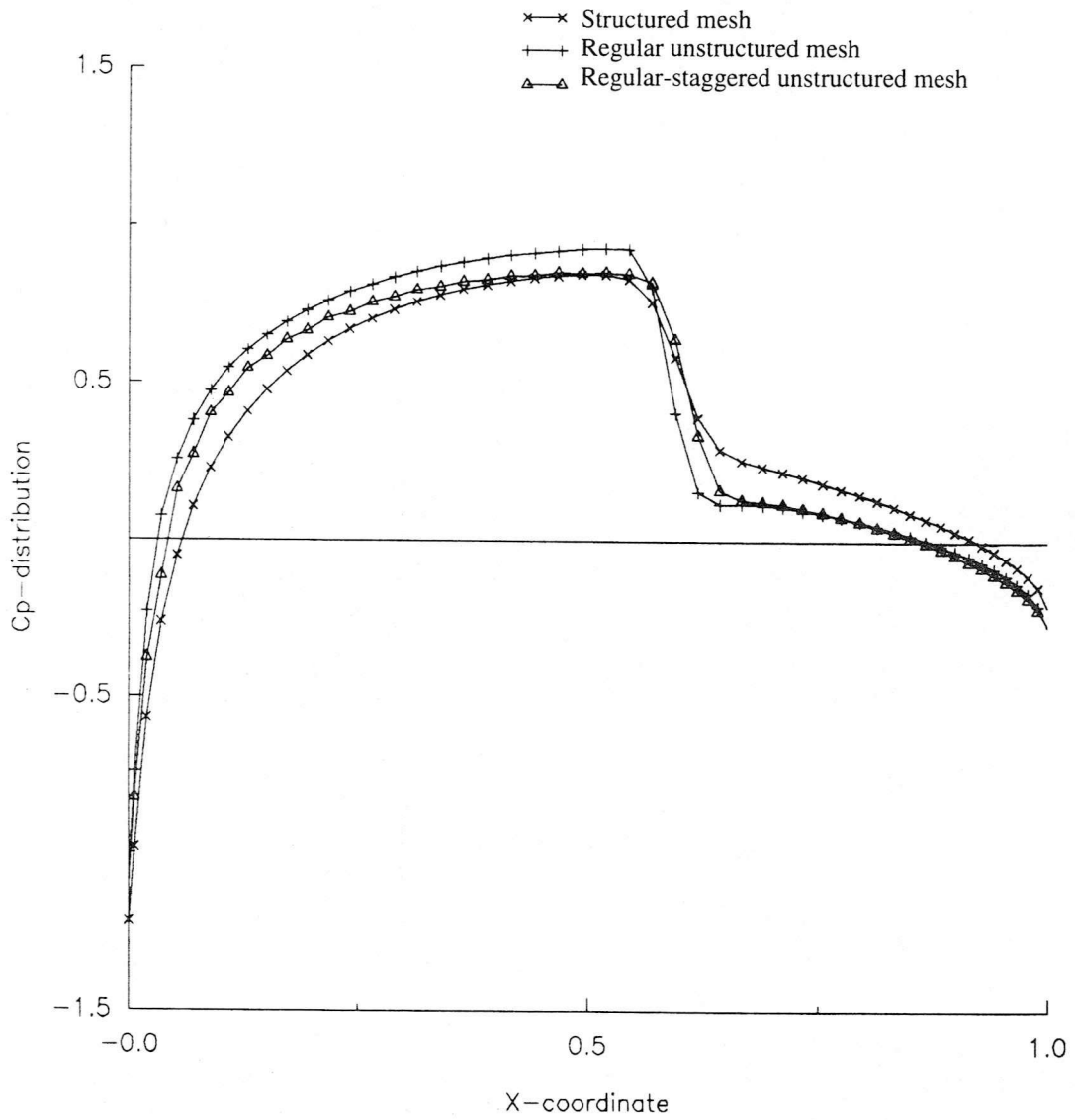

Fig. 5.9 Comparison of pressure coefficient on meshes generated by Eagle package
Mach=0.80 Alp=0.0 deg.

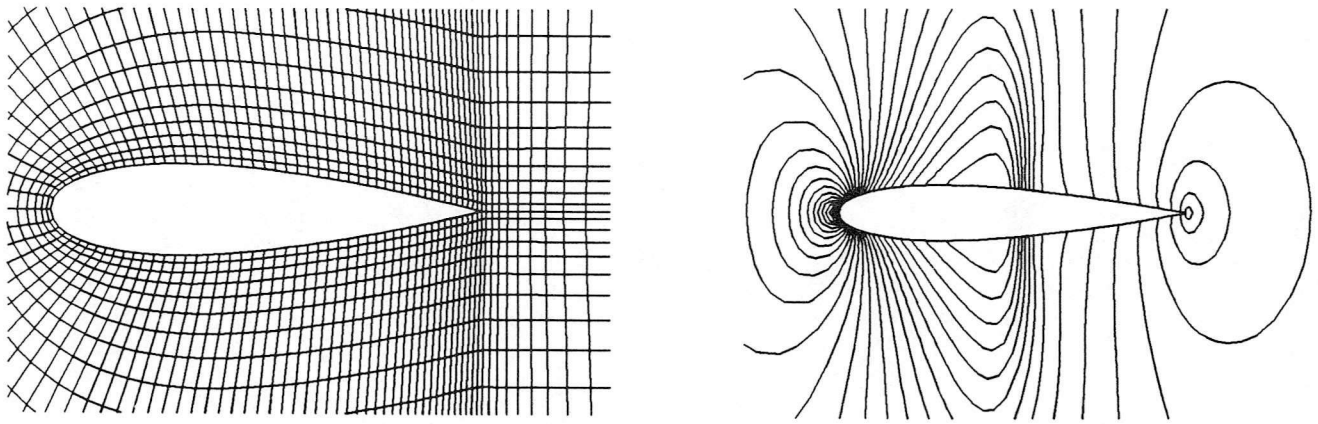

Fig.5.10(a) NACA 0012 airfoil Mesh generator: EAGLE package
Structured mesh: 5120 elements 5313 nodes
Pressure contour: Mach=0.80 Alp=0.0 deg

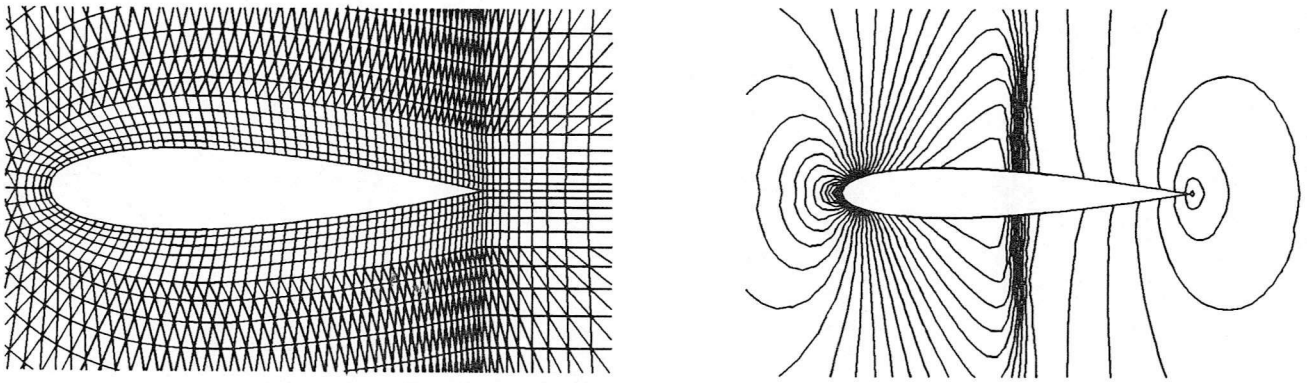

Fig.5.10(b) NACA 0012 airfoil Mesh generator: EAGLE package
Mixed mesh: inner region --- Structured mesh
outer region --- Regular unstructured mesh
total : 9440 elements 5313 nodes
Pressure contour: Mach=0.80 Alp=0.0 deg

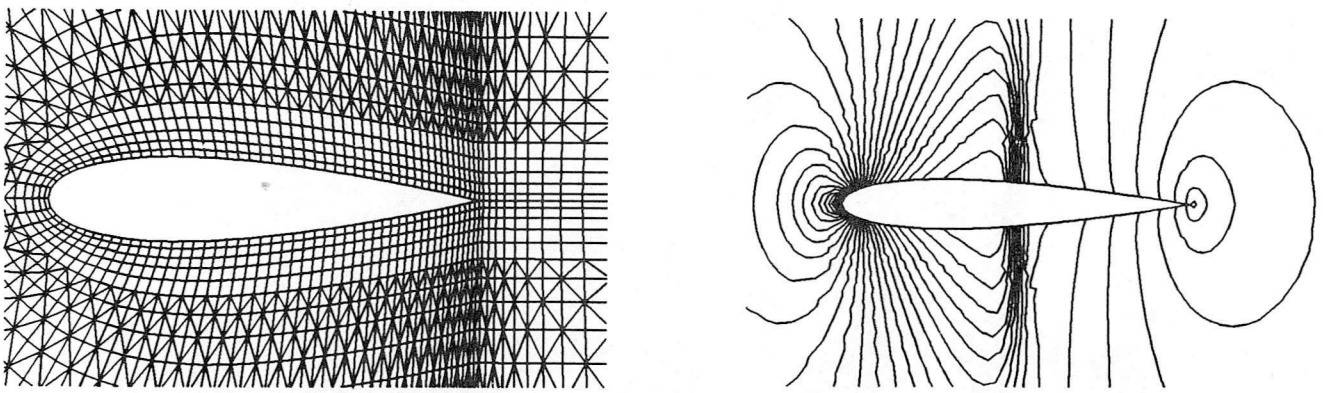

Fig.5.10(c) NACA 0012 airfoil Mesh generator: EAGLE package
Mixed mesh: inner region --- Structured mesh
outer region --- Regular-staggered unstructured mesh
total : 9440 elements 5313 nodes
Pressure contour: Mach=0.80 Alp=0.0 deg

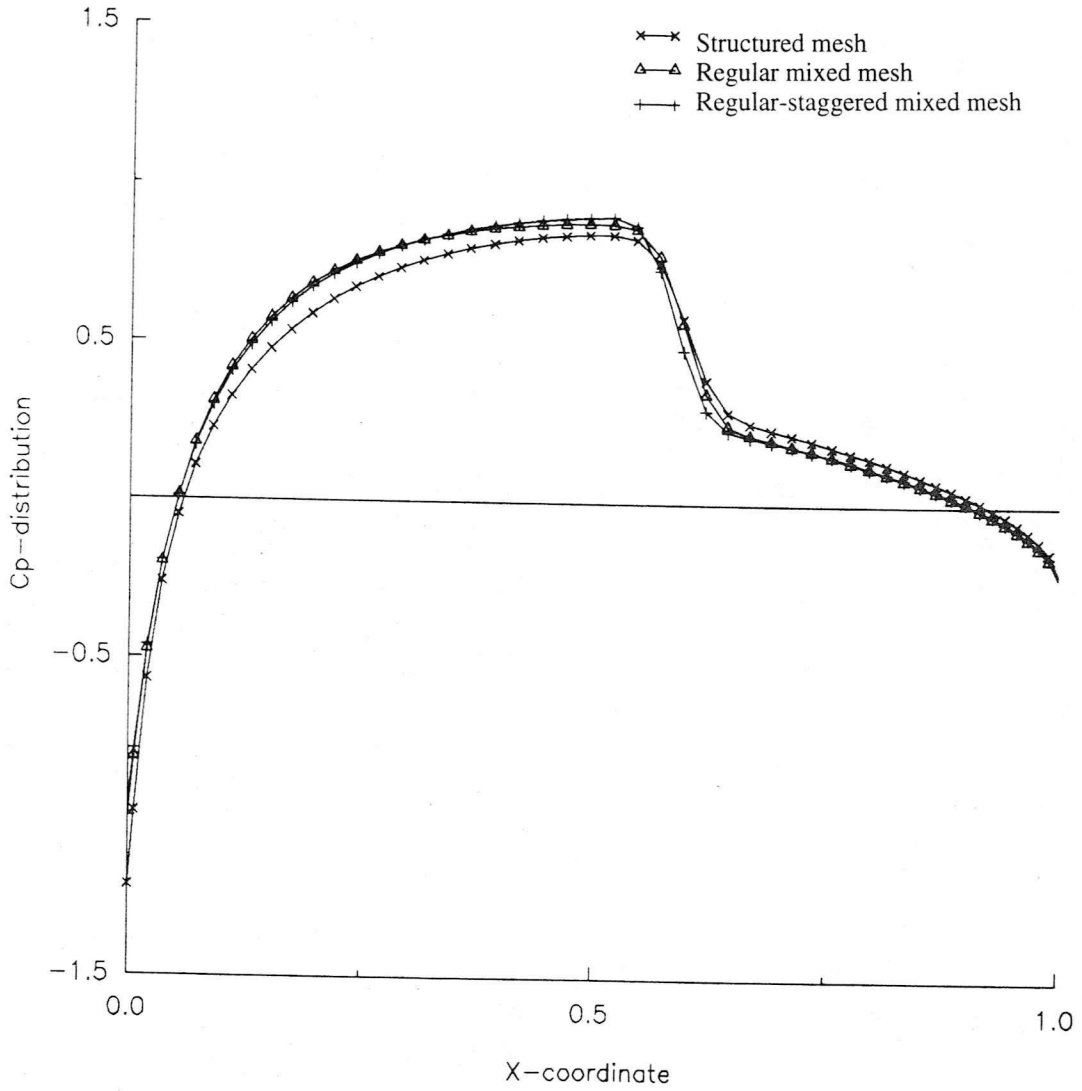

Fig. 5.11 Comparison of pressure coefficient on structured mesh and mixed meshes generated by Eagle package
Mach=0.80 Alp=0.0 deg.

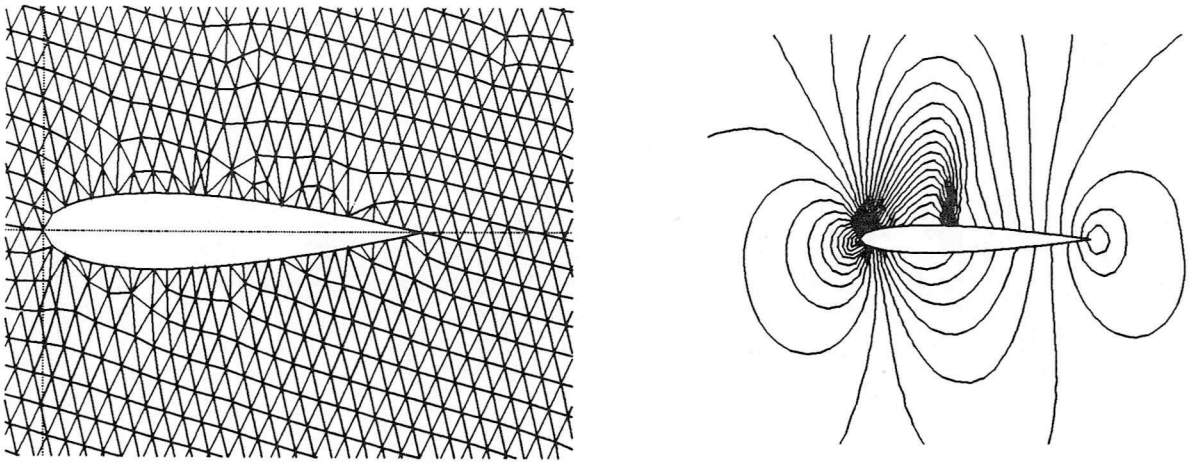

Fig.5.12(a) NACA 0012 airfoil Mesh generator: AFT method
Unstructured mesh: 3246 elements 1670 nodes
Pressure contour: Mach=0.75 Alp=2.0 deg

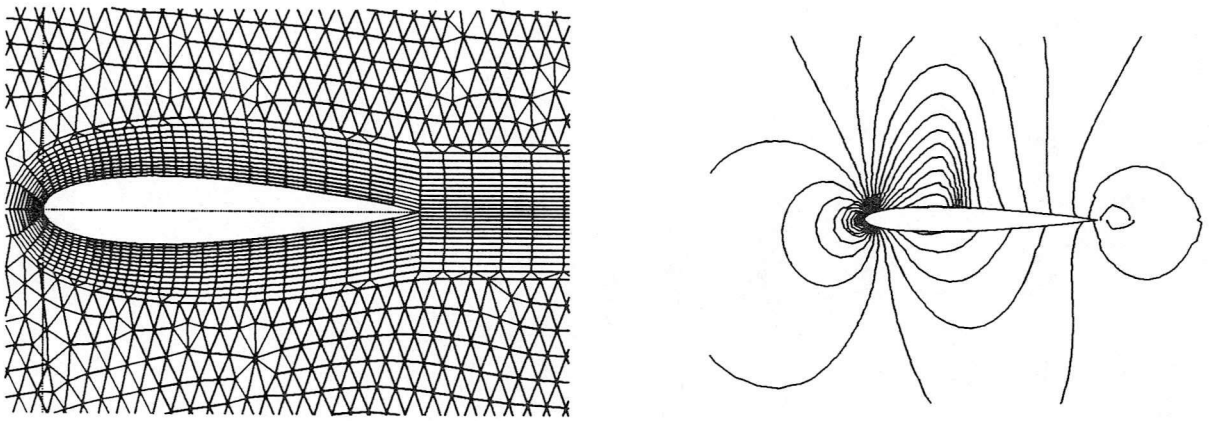

Fig.5.12(b) NACA 0012 airfoil Mesh generator: Hybrid mesh code
Hybrid mesh: inner region --- Structured mesh (ALGEM code)
outer region --- Unstructured mesh (AFT method)
total : 4757 elements 3045 nodes
Pressure contour: Mach=0.75 Alp=2.0 deg

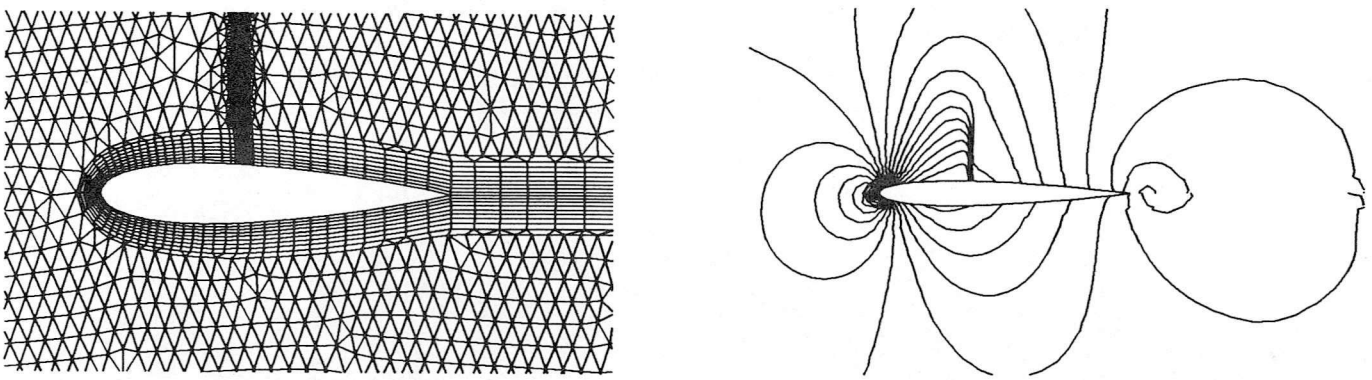

Fig.5.12(c) NACA 0012 airfoil Mesh generator: Hybrid mesh code
Hybrid mesh: inner region --- Structured mesh (ALGEM code)
outer region --- Unstructured mesh (AFT method)
total : 5507 elements 3303 nodes
Pressure contour: Mach=0.75 Alp=2.0 deg

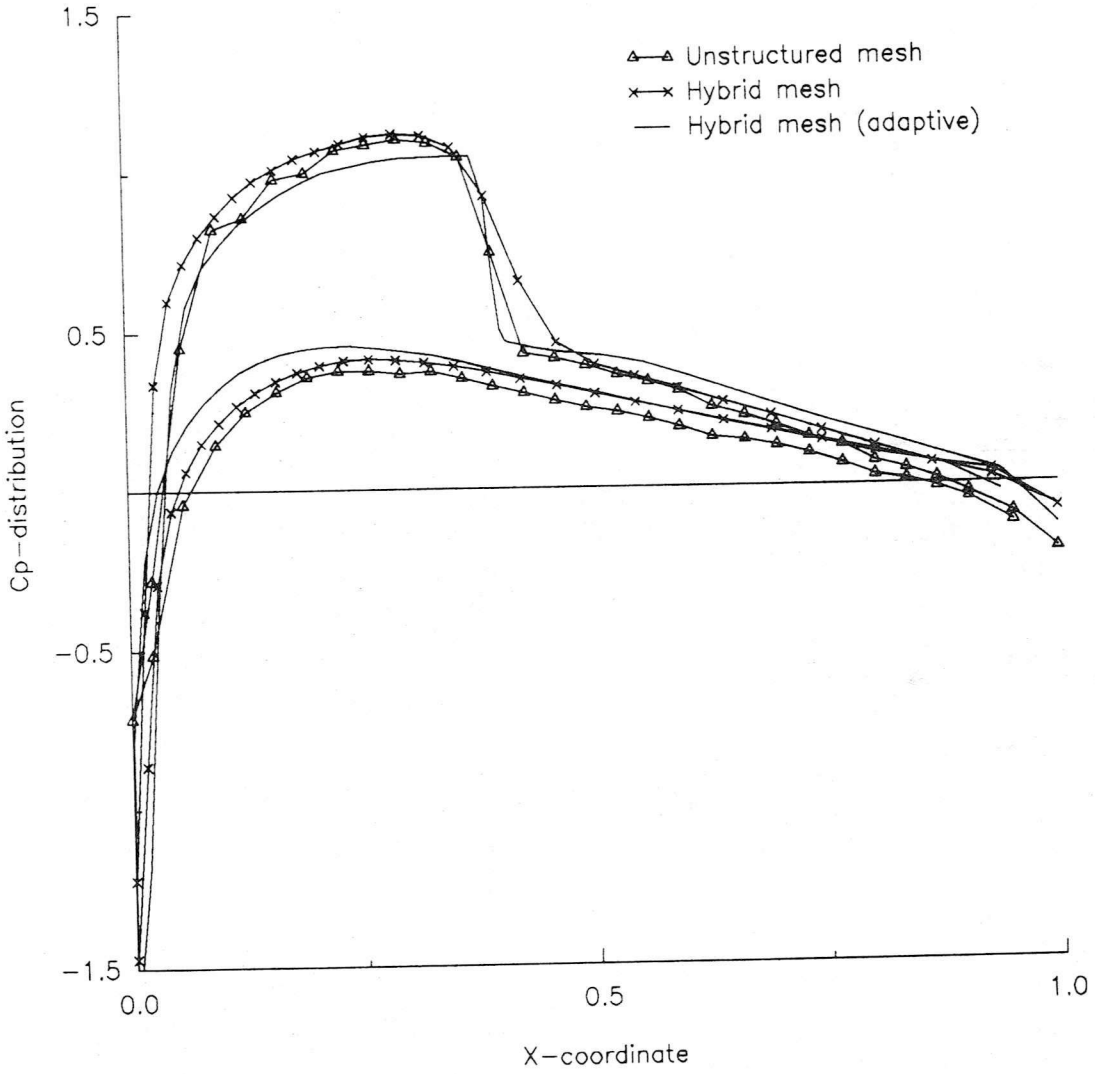

Fig. 5.13 Comparison of pressure coefficient on:
(1) unstructured mesh (AFT)
(2) hybrid mesh (inner region structured mesh by ALGEM code)
(3) adaptive hybrid mesh (inner region structured mesh by ALGEM code)
Mach=0.75 Alp=2.0 deg.

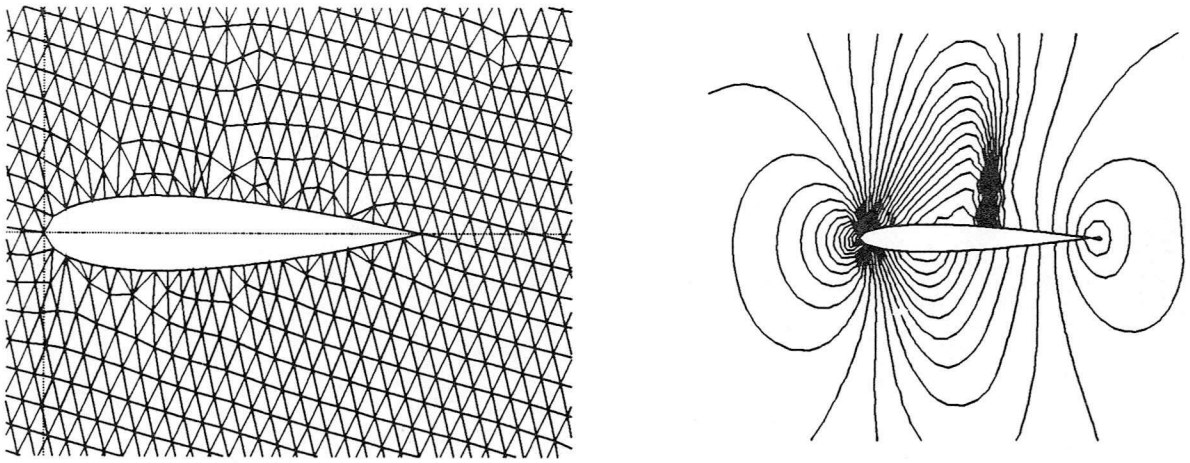

Fig.5.14(a) NACA 0012 airfoil Mesh generator: AFT method
Unstructured mesh: 3246 elements 1670 nodes
Pressure contour: Mach=0.80 Alp=1.25 deg

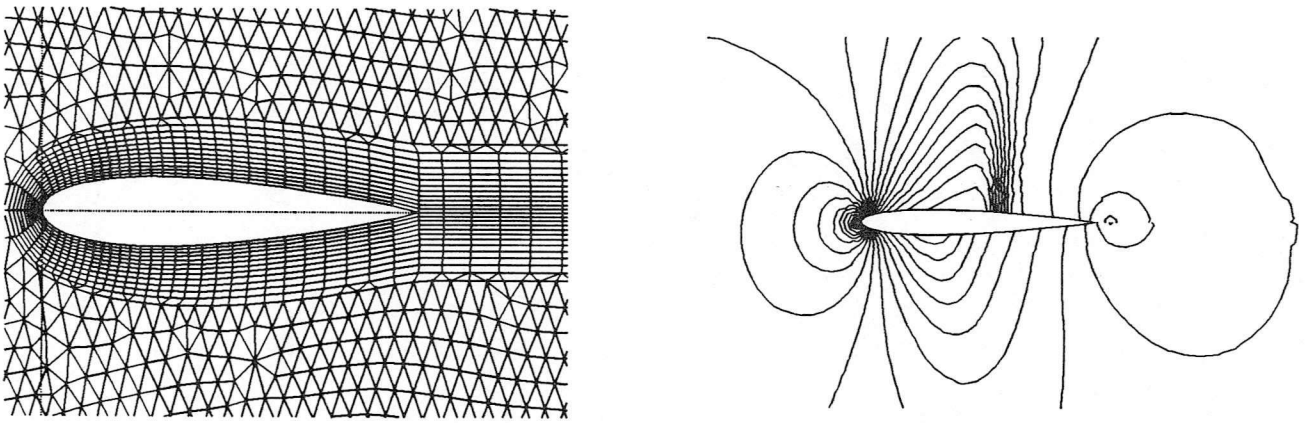

Fig.5.14(b) NACA 0012 airfoil Mesh generator: Hybrid mesh code
Hybrid mesh: inner region --- Structured mesh (ALGEM code)
outer region --- Unstructured mesh (AFT method)
total : 4757 elements 3045 nodes
Pressure contour: Mach=0.80 Alp=1.25 deg

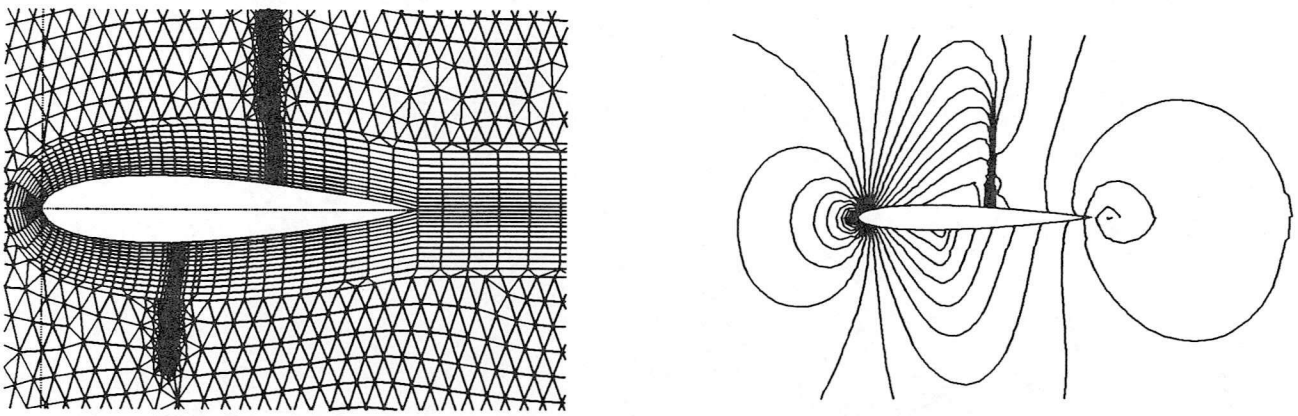

Fig.5.14(c) NACA 0012 airfoil Mesh generator: Hybrid mesh code
Hybrid mesh: inner region --- Structured mesh (ALGEM code)
outer region --- Unstructured mesh (AFT method)
total : 7197 elements 4369 nodes
Pressure contour: Mach=0.80 Alp=1.25 deg

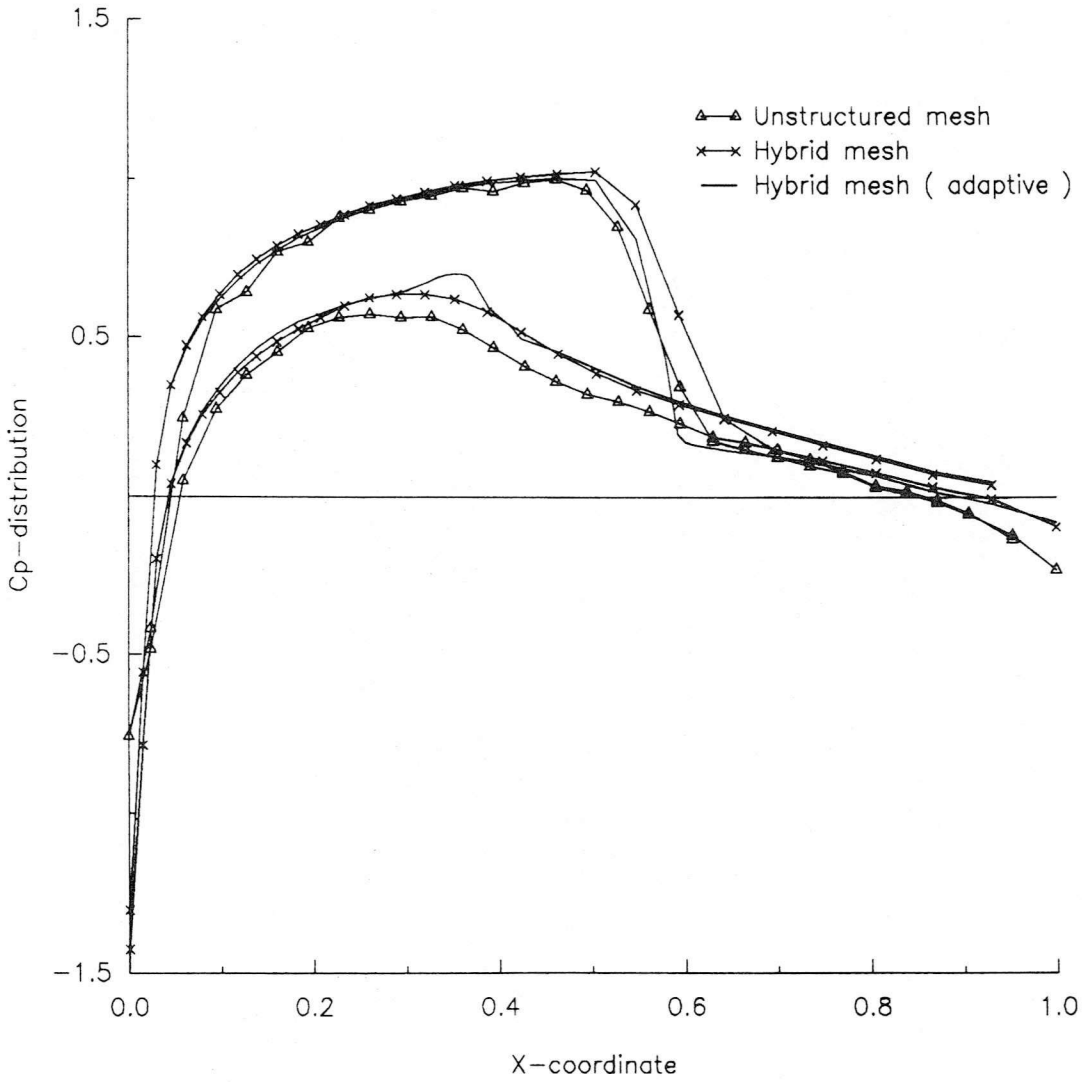

Fig. 5.15 Comparison of pressure coefficient on:
(1) unstructured mesh (AFT)
(2) hybrid mesh (inner region structured mesh by ALGEM code)
(3) adaptive hybrid mesh (inner region structured mesh by ALGEM code)
Mach=0.80 Alp=1.25 deg.

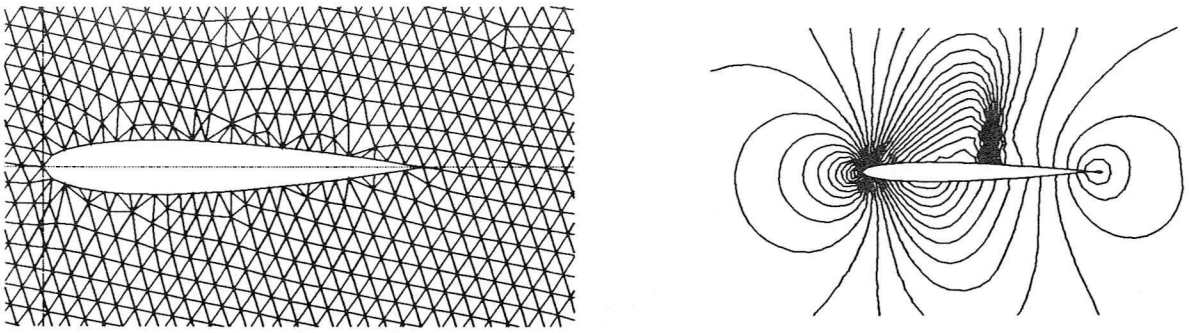

Fig.5.16(a) NACA 0012 airfoil Mesh generator: AFT method
Unstructured mesh: 3246 elements 1670 nodes
Pressure contour: Mach=0.80 Alp=1.25 deg

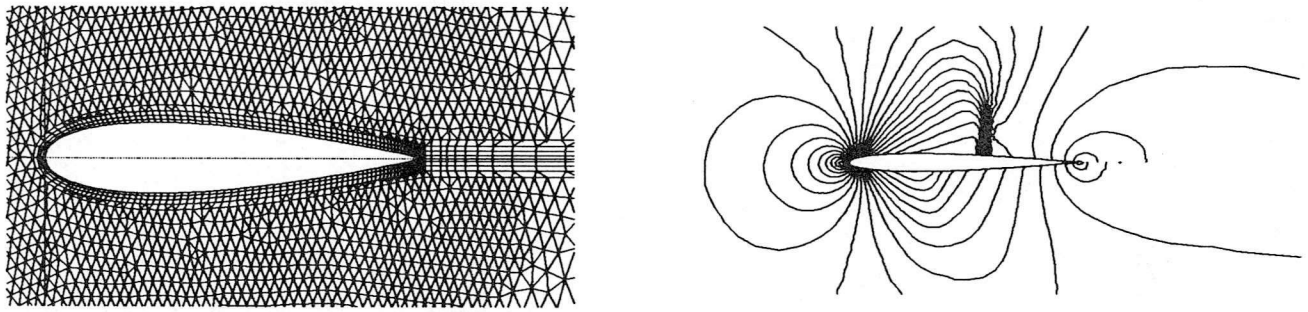

Fig.5.16(b) NACA 0012 airfoil Mesh generator: Hybrid mesh code
Hybrid mesh: inner region --- Structured mesh (EAGLE package)
outer region --- Unstructured mesh (AFT method)
total : 5419 elements 3143 nodes
Pressure contour: Mach=0.80 Alp=1.25 deg

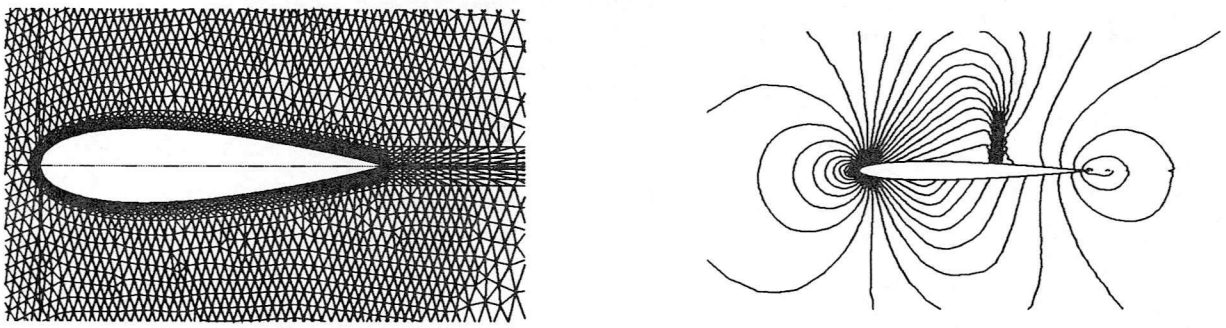

Fig.5.16(c) NACA 0012 airfoil Mesh generator: Hybrid mesh code
Hybrid mesh: inner region --- Regular unstructured mesh (EAGLE package)
outer region --- Unstructured mesh (AFT method)
total : 6057 elements 3143 nodes
Pressure contour: Mach=0.80 Alp=1.25 deg

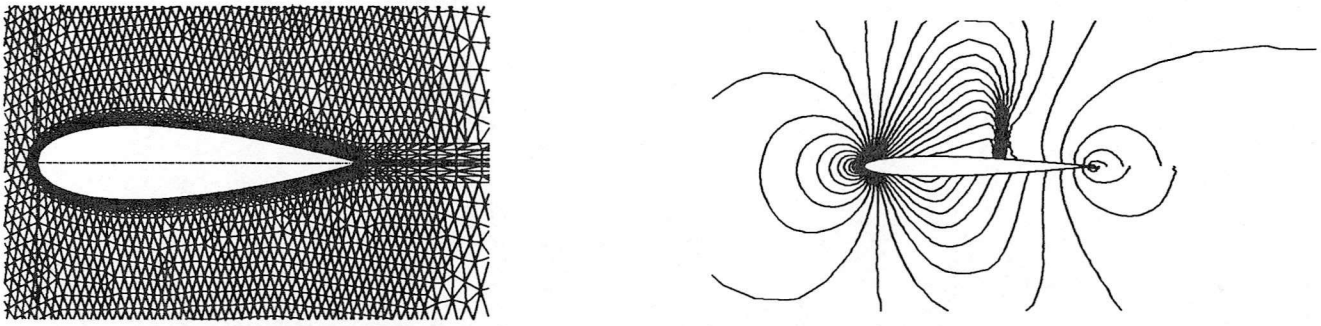

Fig.5.16(d) NACA 0012 airfoil Mesh generator: Hybrid mesh code
Hybrid mesh: inner region --- Regular-staggered unstructured mesh (EAGLE package
outer region --- Unstructured mesh (AFT method)
total : 6057 elements 3143 nodes
Pressure contour: Mach=0.80 Alp=1.25 deg

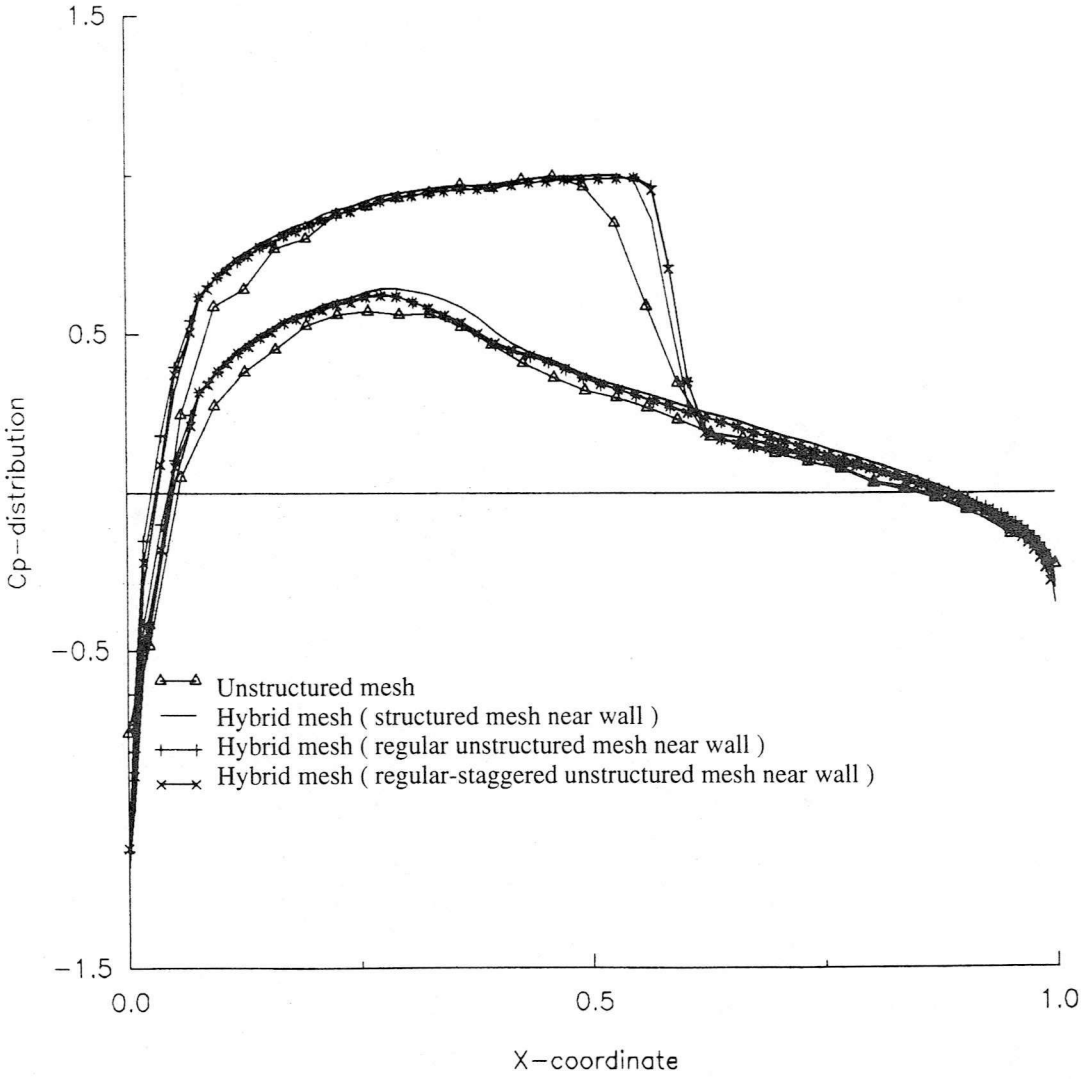

Fig.5.17 Comparison of pressure coefficient on:
(1) unstructured mesh (AFT)
(2) hybrid mesh (inner region structured mesh by EAGLE)
(3) hybrid mesh (inner region regular unstructured mesh by EAGLE)
(4) hybrid mesh (inner region regular-staggered unstructured mesh by EAGLE)